



Dynamically downscaled future projections of the Northwest Atlantic Ocean across low to high emissions scenarios

Dongmin Kim^{1,2}, Andrew C. Ross³, Sang-Ik Shin^{4,5}, Fabian A. Gomez^{6,2}, Jasmin G. John², Denis L. Volkov^{1,2}, Sang-Ki Lee², Michael A. Alexander⁷, and Charles A. Stock³

¹Cooperative Institute for Marine and Atmospheric Studies, University of Miami, Miami, FL, USA

²NOAA/OAR/Atlantic Oceanographic and Meteorological Laboratory, Miami, FL, USA

³NOAA/OAR/Geophysical Fluid Dynamics Laboratory, Princeton, NJ, USA,

⁴Cooperative Institute for Research in Environmental Sciences, University of Colorado Boulder, Boulder, CO, USA

⁵NOAA/OAR/Physical Sciences Laboratory, Boulder, CO, USA

⁶Northern Gulf Institute, Mississippi State University, Starkville, MS, USA

⁷Department of Atmospheric and Oceanic Sciences, University of Colorado Boulder, Boulder, CO, USA

Correspondence: Dongmin Kim (dongmin.kim@noaa.gov)

Received: 23 December 2025 – Discussion started: 6 January 2026

Revised: 29 May 2026 – Accepted: 10 June 2026 – Published: 26 June 2026

Abstract. We used a high-resolution (1/12°) Modular Ocean Model version 6 implementation for the Northwest Atlantic Ocean (MOM6-NWA12) to dynamically downscale Geophysical Fluid Dynamics Laboratory Earth System Model version 4.1 (GFDL-ESM4.1) projections for the 21st century. Simulations were conducted under four different Coupled Model Intercomparison Project Phase 6 emission scenarios. MOM6-NWA12 accurately simulates the spatial patterns of sea surface temperature, salinity, and dynamic sea surface height (SSH) during the historical period. In particular, the Gulf Stream’s strength, position, recirculation, and separation from the US East Coast are significantly improved in MOM6-NWA12 compared to the coarse-resolution GFDL-ESM4.1. Projected end-of-century warming varied strongly between scenarios, from $\sim 4^\circ\text{C}$ under prior “worst case” emissions scenarios (SSP-585), $2 \sim 3^\circ\text{C}$ under intermediate scenarios (SSP-245, SSP-370) more consistent with current trajectories, to $\sim 1^\circ\text{C}$ under aggressive mitigation (SSP-126). Consistent with a significant weakening of the Atlantic Meridional Overturning Circulation projected by GFDL-ESM4.1, MOM6-NWA12 shows a substantial volume transport reduction in the Western Boundary Current (WBC) system (i.e., Yucatan Current, Florida Current, Antilles Current, and the Deep Western Boundary Current) toward the late 21st century (between 23 % and 38 %, varying by scenario). This projected weakening of the WBC system

and the associated reduction in the coastal upwelling of cold, fresh subsurface waters lead to a significant increase in ocean temperature, salinity, and dynamic SSH along the US south-east and northeast Coasts, particularly in the South Atlantic Bight.

1 Introduction

The Northwest Atlantic Ocean (NWA), including the United States (US) East and Gulf Coasts, and the Caribbean Sea, is characterized by large spatial heterogeneity in ocean conditions and complex interactions between ocean circulation and biogeochemistry (e.g., Wang et al., 2013; Muller-Karger et al., 2015; Wanninkhof et al., 2015; Gomez et al., 2020; 2022; Friedrichs et al., 2019; Zhang et al., 2023). A myriad of living marine resources inhabit this region, including the South Florida coral reefs, lobsters and shellfish, demersal fish species like groupers, snappers, cod and haddock, and migratory pelagic fish species like bluefin tuna and king mackerel, all of whose distribution and abundance are influenced by changes in ocean temperature and circulation (e.g., Weinberg 2005; Bell et al., 2015; Karnauskas et al., 2013, 2015; Tanaka et al., 2020). Previous studies have shown that portions of the ocean ecosystem are modulated by large scale climate variability, such as El Niño Southern Oscillation and At-

lantic Multidecadal Oscillation, through associated changes in ocean circulation and river runoff (e.g., Alexander and Scott, 2008; Gomez et al., 2019, 2024). Moreover, the region is undergoing sustained warming, particularly along the US South and East Coasts, where the surface temperature warming rate was about two or three times faster than that of the global ocean average for 1970–2020 (e.g., Pershing et al., 2015; Wang et al., 2023).

Previous studies have also attributed regional acceleration and spatial variation of the US East Coast sea level rise to ocean circulation changes, including a weakening of the Gulf Stream (e.g., Ezer et al., 2013; Ezer, 2015; Goddard et al., 2015; Park and Sweet, 2015; Dong et al., 2019), warming of the Gulf Stream and the entire subtropical gyre (e.g., Domingues et al., 2018; Volkov et al., 2019, 2023; Steinberg et al., 2024; Huang et al., 2025), and a slowdown of the Atlantic Meridional Overturning Circulation (AMOC, e.g., Levermann et al., 2005; Little et al., 2017, 2019). While progress has been made in understanding ocean conditions off the US East and Gulf Coasts and in the Caribbean Sea, substantial uncertainties still remain regarding future changes in regional ocean circulation and their sensitivity to greenhouse gas emissions scenarios. Consequently, it is essential to investigate projected changes in ocean circulation across scenarios to improve our understanding of future ocean conditions and ecosystem dynamics across the Northwest Atlantic.

Global models, such as General Circulation models (GCMs) and Earth System Models (ESMs), offer valuable insights into future ocean conditions under various climate scenarios. However, they are often limited in spatial resolution due to computational constraints and may face significant uncertainties due to limitations in representing the fine-scale ocean circulation and thermohaline structures, particularly in coastal regions. Hence, high-resolution, eddy-resolving ocean models are critical for addressing these limitations, providing improved representations of historical ocean circulation across multiple timescales and offering more reliable future projections (e.g., Drenkard et al., 2021). To leverage the benefits of resolving eddies and shelf-scale circulation while lowering the computational burden, multiple studies have applied dynamic downscaling techniques to better understand and project regional impacts of climate change on NWA ocean systems (e.g., Liu et al., 2012, 2015; Alexander et al., 2020; Shin and Alexander, 2020; Rutherford et al., 2024).

By refining the outputs of GCMs/ESMs using high-resolution regional models, dynamical downscaling can capture finer-scale processes and interactions that are often missed by coarse-resolution models. For example, the projected weakening of the Loop Current and associated reduction in warm water transport through the Yucatan Channel are poorly resolved in Coupled Model Intercomparison Project Phase 5 (CMIP5) and CMIP6 global models, leading to an overestimation of SST warming over the northern part of the

Gulf of America (GoA; a.k.a. Gulf of Mexico) and underestimation of SST warming along the West Florida shelf – an issue better addressed by high-resolution downscaled models (e.g., Liu et al., 2012, 2015). Similarly, systematic CMIP model biases in the Gulf Stream representation led to underestimation of warming of Northeast US waters associated with future changes in the Gulf Stream path (Saba et al., 2016).

In line with these efforts, the National Oceanic and Atmospheric Administration (NOAA) Changing Ecosystems and Fisheries Initiative (CEFI) modeling team has developed a high-resolution regional ocean model – the Modular Ocean Model version 6 at $1/12^\circ$ horizontal resolution (~ 8 km) for the Northwest Atlantic Ocean (MOM6-NWA12; Ross et al., 2023). MOM6-NWA12 is configured to capture key regional features and simulate ocean dynamics in the Northwest Atlantic with high fidelity. This model provides a valuable framework for studying the complex interactions between large-scale processes and local features that govern both physical and biogeochemical variability in the region. MOM6-NWA12 demonstrates strong performance in reproducing a broad range of observed physical and biogeochemical conditions during the hindcast period (1993–2020, Ross et al., 2023). Furthermore, it exhibits skillful seasonal to decadal forecast capabilities for SST anomalies (SSTAs, Koul et al., 2024; Ross et al., 2024). However, while MOM6-NWA12 has shown promise for seasonal and decadal predictions, its potential for multi-decadal (30 \sim 100 years) projections remains unexplored.

In this study, we use the high-resolution MOM6-NWA12 model to dynamically downscale future projections from the Geophysical Fluid Dynamics Laboratory's Earth System Model version 4.1 (GFDL-ESM4.1) for the Northwest Atlantic Ocean. With this downscaling procedure, we aim to generate more accurate and regionally relevant projections of future ocean conditions. Unlike prior studies, which used a single greenhouse gas emissions scenario, we consider the range of potential ocean futures from projections using four different scenarios (i.e., Shared Socioeconomic Pathways; SSP-126, SSP-245, SSP-375, and SSP-585) spanning aggressive mitigation to high emissions pathways beyond our current trajectory. This allows us to identify the NWA responses to future climate change that are sensitive to emissions pathways from those that are not, and to explore mechanisms underlying these contrasts. We also build on prior work to understand regional hot-spots of ocean change and their drivers. This approach enhances our understanding of regional ocean dynamics and supports the development of effective mitigation and adaptation strategies in response to climate change.

2 Model and downscaling settings

2.1 MOM6-NWA12

MOM6-COBALT-NWA12 is a coupled ocean circulation and sea ice model which can also include coupled ocean biogeochemistry (Ross et al., 2023). Here, we consider a “physics-only” implementation of this system (i.e., MOM6-NWA12), which has also been applied for seasonal and decadal prediction applications (Ross et al., 2024; Koul et al., 2024). The model spans the Northwest Atlantic Ocean, including the Caribbean Sea, the Gulf Coast, and the US East Coast 98–36° W and 5–52° N, and has 775 × 845 grid points (Fig. 1). The nominal horizontal resolution is about 1/12°. The zonal distance between grid points varies with latitude, from ~ 9 km at the southern boundary to ~ 5 km at the northern boundary. The model has 75 vertical layers using a z^* -coordinate, a depth coordinate rescaled with the free surface (Adcroft and Campin, 2004). The vertical resolution is finest near the surface, where the layer thickness is 2 m, increasing gradually with depth to a maximum thickness of 250 m above the deepest model depth of 6500 m. The model’s subgrid-scale parameterizations are adapted from the 1/4° global MOM6, with updates and modifications to account for the increased horizontal resolution (Ross et al., 2023). MOM6-NWA12 has the option of using time steps for thermodynamics and ocean-biogeochemistry longer than the baroclinic time step, which significantly reduces the running time for coupled model simulations. More detailed model description, additional features, and parameterization settings can be found in Ross et al. (2023).

2.2 GFDL-ESM4.1

NOAA GFDL’s Earth System Model version 4.1 (GFDL-ESM4.1, Dunne et al., 2020) provides the boundary conditions for the MOM6-NWA12 simulations. We carried out four sets of MOM6-NWA12 simulations downscaling GFDL-ESM4.1 simulations under SSP-126, SSP-245, SSP-375, and SSP-585 scenarios (O’Neill et al., 2016). GFDL-ESM4.1 is built on a basis of GFDL’s AM4.0 atmospheric model, which has 49 hybrid vertical layers and approximately 1° × 1° horizontal resolution (Zhao et al., 2018a, b), using the Finite Volume version 3 (FV3; Lin, 2004) dynamical core with advanced parameterizations of moist convection, clouds, radiation, topographical drag, and several other physical processes from its previous version. The land model in GFDL-ESM4.1 is GFDL’s Land Model version 4.1 (LM4.1; Shevliakova et al., 2024), which improved radiative properties for vegetation, soil, and snow, and updated hydrology in LM4.0. The ocean model component of GFDL-ESM4.1 uses MOM6 (Adcroft et al., 2019), configured with a nominal resolution of 1/2° horizontally and 75 vertical hybrid z^* -coordinate layers within the Arbitrary-Lagrangian-Eulerian algorithm (Adcroft and Hallberg, 2006), and the

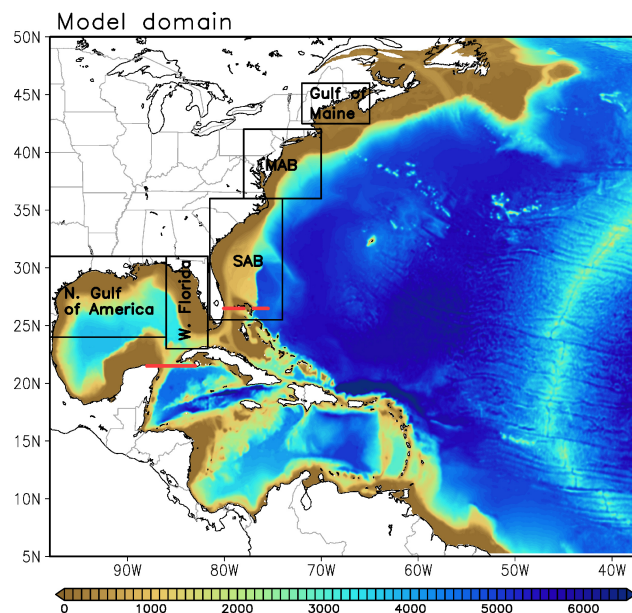


Figure 1. MOM6-NWA12 model domain and bathymetry (m). The black boxes indicate the location of the Northern Gulf of America, West Florida, South Atlantic Bight (SAB), and middle Atlantic Bight (MAB), and Gulf of Maine for exploring sea-level rise. The red solid lines are the locations of four major Northwestern Atlantic boundary current systems (Yucatan Current, Florida Current, Antilles Current (0 ~ 500 m), and Deep Western Boundary Current (1000–4000 m)).

GFDL’s Sea Ice Simulator (SIS2; Adcroft et al., 2019). More detailed model description, additional features, and parameterization settings of GFDL-ESM4.1 can be found in Dunne et al. (2020). It is noted that the equilibrium climate sensitivity (ECS) of GFDL-ESM4 is approximately 2.6 K, which is at the lower end of the sensitivity range for CMIP6 models (Dunne et al., 2020; Meehl et al., 2020; Sentman et al., 2026).

2.3 Reanalysis datasets

The global reanalysis datasets used to force the retrospective ocean simulation of Ross et al. (2023) are also used here for bias corrections of ocean lateral boundary conditions, surface forcings, and river discharge for the historical and future projections derived from GFDL-ESM4.1 (Table 1). We use the high-resolution (1/12°) Global Ocean Physics Reanalysis (GLORYS12; Lellouche et al., 2021) to derive monthly ocean temperature, zonal and meridional speeds of ocean current, salinity, and sea surface height (SSH) for 1993–2020 period. We also use 3 hourly European Centre for Medium-Range Weather Forecast (ECMWF) Reanalysis version 5 (ERA5) atmospheric reanalysis datasets to derive near-surface zonal and meridional winds, near-surface air temperature, specific humidity, precipitation, and downwelling short- and long-wave radiative fluxes (Hersbach et al., 2020).

Table 1. Reanalysis products and associated variables used for the bias correction and validation in this study.

Reanalysis product	Variables	Frequency
ERA5	2 m temperature	3 hourly
	2 m specific humidity	3 hourly
	10 m zonal wind	3 hourly
	10 m meridional wind	3 hourly
	Sea level pressure	Daily
	Liquid precipitation rate	Daily
	Snowfall rate	Daily
	Downward shortwave radiative flux	Daily
	Downward longwave radiative flux	Daily
GLORYS12	Sea water potential temperature	Monthly
	Sea water salinity	Monthly
	Sea water zonal velocity	Monthly
	Sea water meridional velocity	Monthly
	Sea surface height	Monthly
GloFAS	River runoff rate	Daily

For river discharge, we use the gridded daily Global Flood Awareness System (GloFAS) version 3.1 reanalysis (Alfieri et al., 2020). Although global river discharge driven by climate change exhibits a clear positive trend, the projected changes in river discharge in our regional model domain (i.e., the southern and eastern US seaboard) are insignificant and uncertain during the first half of the 21st century (Muller et al., 2024). Therefore, we did not consider future changes in runoff in this single-model downscaling and instead applied the daily mean climatology (1993–2020) of GloFAS river runoff data for the entire simulation period (1950–2100). As a result, the potential effects of regional runoff change on nearshore salinity and sea level are not addressed in this study.

2.4 Mean bias correction

To reduce systematic biases in the GFDL-ESM4 outputs, we applied a climatological mean bias correction to the lateral ocean boundary conditions (BCs) and surface atmospheric forcing fields using the GLORYS12 and ERA5 reanalysis datasets as follows:

$$\text{Bias-corrected variables} = \text{GFDL-ESM4} + \text{Delta}$$

$$\text{Delta} = \langle \text{Reanalysis} \rangle - \langle \text{GFDL-ESM4} \rangle$$

where the GFDL-ESM4 refers to the raw outputs from the GFDL-ESM4 simulations. $\langle \text{Reanalysis} \rangle$ and $\langle \text{GFDL-ESM4} \rangle$ are the long-term averaged annual cycles from the reanalysis and GFDL-ESM4 simulations for the 1993–2020 period, respectively. For the GFDL-ESM4 simulations, we merged the data from its historical simulation (1993–2014) with the data from the future period in each of the four SSP scenarios (2015–2020). The long-term (1993–2020) means for

each month of the year determine the mean annual cycle of the ocean variables, while the long-term means for each 3 hourly period of the year determine the mean annual cycle of the atmospheric variables. The mean bias correction terms, Delta, were then added to the GFDL-ESM4 outputs for the entire simulation period (1950–2100) to correct the mean biases. This bias correction method ensures that mean states of MOM6-NWA12 during the historical period (1993–2020) are comparable to those in the reanalysis datasets and in Ross et al. (2023).

It is noted that our “Delta method” shares similarities with approaches from previous studies (Liu et al., 2012; 2015; Alexander et al., 2020; Shin and Alexander, 2020; Pozo Buil et al., 2021), which replace model climatology with reanalysis climatology to reduce mean biases. However, our method fundamentally differs in its treatment of high-frequency atmospheric forcing. While those previous studies utilized high-frequency atmospheric forcing (i.e., daily time scales) from historical reanalysis datasets for future projections - thereby assuming that high-frequency forcing remains unchanged in the future - we retained the model-generated high-frequency atmospheric variability (e.g., 3 hourly and daily). We took this approach to ensure more consistent climate projections, recognizing that weather and climate are interdependent. Indeed, not only does weather depend strongly on low-frequency variability (e.g., weather conditions during the different phases of ENSO are substantially different), but also weather statistics can substantially change under future climate conditions (e.g., Cheng et al., 2012; Jeong and Sushama, 2019).

A second notable difference between the methodology herein and past Northwest Atlantic downscaling studies is the replacement of limited “time slice” experiments with a continuous integration over the historical and future periods. The continuous integration approach requires more computational investment (time slices were generally compared across 10–30 year intervals while continuous integrations required 150 years), but it allows for a more complete analysis of the emergence of significant differences between scenarios and historical conditions, and between the scenarios themselves (e.g., Drenkard et al., 2021).

Finally, for sea level, we note that both GFDL-ESM4.1 and MOM6-NWA12 utilize the Boussinesq approximation, which conserves ocean volume. The dynamic sea level in both models can respond to local density changes driven by local warming and freshening (e.g., Steinberg et al., 2024). However, these models cannot simulate global mean sea-level (GMSL) rise caused by thermosteric expansion or added mass from ice melt (e.g., Greatbatch, 1994; Griffies and Greatbatch, 2012; Griffies et al., 2014). Furthermore, to prevent potential drifts in the basin-integrated water volume associated with the lateral open boundary conditions, we explicitly constrain the basin-averaged SSH anomaly to be zero throughout all MOM6-NWA12 simulations. Consequently, the SSH changes derived from MOM6-NWA12 strictly rep-

resent the dynamic redistribution of water mass driven by regional ocean circulation and local steric adjustments.

3 Results

3.1 Model validation for the historical period

To evaluate the performance of GFDL-ESM4.1 and MOM6-NWA12 in the historical period, we first compared model-derived climatologies of SST, sea surface salinity (SSS), and surface current speed against the GLORYS12-derived climatological patterns (Figs. 2 and S1 in the Supplement). The GFDL-ESM4.1 outputs show considerable biases in the SST and SSS mean patterns. Specifically, the SST has a warm bias $> 3^{\circ}\text{C}$ in the Mid-Atlantic Bight (MAB), and a cold bias $> 2^{\circ}\text{C}$ in magnitude along the North Atlantic Current path compared to the data-assimilative GLORYS12 product (Fig. 2d). GFDL-ESM4.1 SSS is saltier than the GLORYS SSS over the entire domain (Fig. 2e), especially in the MAB and along the US Gulf Coast, where the bias reaches values $> 3\text{PSU}$. These biases are greatly reduced in the MOM6-NWA12. For example, the SST biases in the MAB and along the Gulf Stream are $\sim 1^{\circ}\text{C}$ or lower (Fig. 2g). The SSS shows a small negative bias, except over the Gulf of Maine, where SSS is overestimated by about 0.7 PSU (Fig. 2h).

The bias patterns for surface ocean velocity reveal that ESM4.1's Loop Current is more diffusive and extended more northward compared to that in GLORYS12 (Figs. 2f and S1c). This appears to be due to the coarse horizontal resolution of GFDL-ESM4.1 ($\sim 0.5^{\circ}$), which is not fine enough to resolve the Loop Current dynamics (e.g., Liu et al., 2012, 2015). In addition, ESM4.1's Gulf Stream along the South Atlantic Bight (SAB) is weaker and slightly shifted away from the US East Coast compared to that in GLORYS12 (Fig. S2). In contrast, MOM6-NWA12 shows much improvement of both the Loop Current and Gulf Stream System (Figs. 2i and S1f). For instance, the Florida Current (beginning of the Gulf Stream System) in MOM6-NWA12 flows closer to the coastline compared to that in GFDL-ESM4.1 with speeds exceeding 1 m s^{-1} , a pattern similar to GLORYS12 (Fig. 2f and i).

After the separation of the Gulf Stream from the US East Coast, the sluggish flow in GFDL-ESM4.1 is shifted northward compared to GLORYS12, both at its separation point and as it travels eastward across the North Atlantic (Fig. 2f). In contrast, the faster Gulf Stream in MOM6-NWA12 (Fig. 2i) is shifted southward at its separation from the coast before regaining consistency with the data-assimilative GLORYS12 path to the east. This is more clearly shown in Fig. S2, which shows the position of the Gulf Stream core as a 15°C isotherm at 200 m (e.g., Sanchez-Franks and Zhang, 2015; Hameed et al., 2018; Seidov et al., 2021; Ross et al., 2023). A northward shift in the Gulf

Stream position is typical in low-resolution ocean models and has been attributed to misrepresentation of nonlinear vorticity boundary dynamics. While it is not clear why the Gulf Stream in MOM6-NWA12 is shifted southward, previous studies have indicated that the separation of the Gulf Stream in an eddy-resolving model is very sensitive to the choices made for subgrid scale parameterizations (e.g., Chassignet and Marshall, 2008).

Consistent with the surface current speed and position of the Gulf Stream, GFDL-ESM4.1 displays a large negative bias in the dynamic sea surface height (SSH), immediately south of the Gulf Stream core and its extension to the North Atlantic Current. Connected with this, the recirculation gyre south of the Gulf Stream (35°N – 73°W), known as the Worthington Gyre (Worthington, 1976), is almost completely absent in GFDL-ESM4.1 (Fig. 3b and d). On the other hand, the spatial pattern of the dynamic SSH in MOM6-NWA12 exhibits improved agreement with that in GLORYS12 (Fig. 3c and e), reproducing a Worthington Gyre albeit weaker than GLORYS12. Given that the Worthington Gyre is a long-term mean rectification of the Gulf Stream rings and instability waves not resolved at coarse resolution, it is not surprising that the recirculation gyre is better represented in MOM6-NWA12 while it is nearly absent in GFDL-ESM4.1.

Lastly, we evaluated the volume transports of Northwestern Atlantic boundary current systems across four zonal transects for the Yucatan Current, Florida Current, Antilles Current, and the Deep Western Boundary Current (DWBC), which are key components of AMOC (McCarthy et al., 2015), as shown in Fig. 4. The zonal transection lines for the four current systems are shown in Fig. 1 (red solid lines). The Antilles Current transport was obtained by integrating the meridional flow over the upper 500 m across 26.5°N and 77.5 – 75°W . Similarly, the DWBC transport was obtained by integrating the meridional velocity between 1000 and 5000 m across 26.5°N and 77.5 – 75°W . GFDL-ESM4.1 simulates a Yucatan Current transport of $43.9 \pm 2.87\text{ Sv}$, which is about 62 % larger than in-situ observation of $27.5 \pm 2.6\text{ Sv}$ (Athié et al., 2015, 2020, Fig. 4a). In contrast, MOM6-NWA12 simulates a transport of $24.2 \pm 1.7\text{ Sv}$, which agrees much better with the observed transport. However, the Florida Current (80 – 77.5°W) transport simulated by MOM6-NWA12 ($24.3 \pm 1.6\text{ Sv}$) underestimates the observation ($32.5 \pm 3.2\text{ Sv}$ in Volkov et al., 2024), whereas the Florida Current transport simulated by GFDL-ESM4.1 ($34.4 \pm 2.5\text{ Sv}$) is comparable to the observation. This occurs despite far more realistic surface current speeds in MOM6-NWA12 (i.e., Fig. 2f and i) because the GFDL-ESM4.1 Florida Current is far more diffusive and extends to greater depth. Additional sensitivity simulations indicate that the Florida Current transport in MOM6-NWA12 is quite sensitive to the eddy viscosity (not shown). By increasing the model diffusivities in MOM6-NWA12, the simulated Florida Current transport also increased closer to the observed value. However, this occurred at the expense of other model features, such as the latitude of Gulf Stream sep-

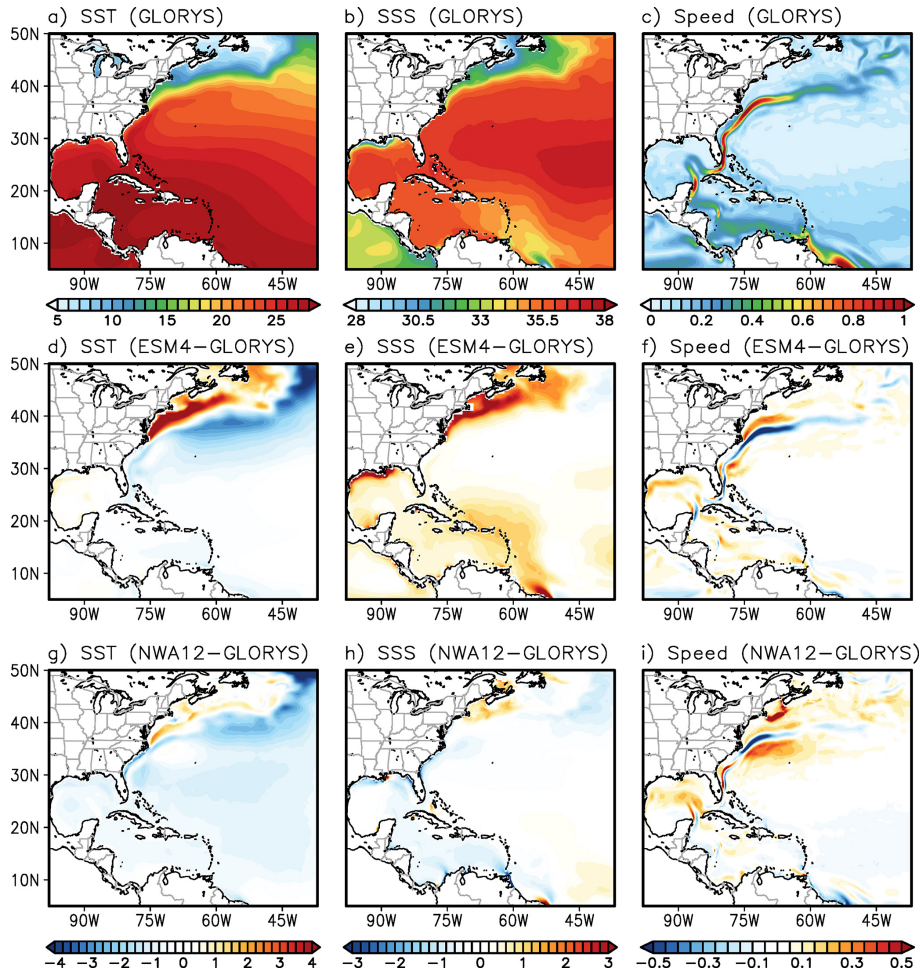


Figure 2. Spatial patterns of the historical (1993–2020) mean (a) sea surface temperature (SST, °C), (b) sea surface salinity (SSS, PSU), and (c) surface current speed (m s^{-1}) in GLORYS12. (d–f) show the GFDL-ESM4.1 biases for SST, SSS, and surface current speed. (g–i) are the same as (d–f), but for MOM6-NWA12.

aration from the coast, becoming less realistic. Therefore, the momentum and density diffusivities for MOM6-NWA12 are unchanged from those used in Ross et al. (2023).

As shown in Fig. 4c and d, the simulated transports for both the Antilles Current ($12.3 \pm 4.1 \text{ Sv}$) and the DWBC ($-20.8 \pm 8.8 \text{ Sv}$) in the GFDL-ESM4.1 show substantial disagreement with observations ($4.7 \pm 5.2 \text{ Sv}$ for the Antilles Current, Meinen et al., 2019; and $-31.2 \pm 5.5 \text{ Sv}$ for the DWBC, Zantopp et al., 2017). MOM6-NWA12, in contrast, better reproduced both the Antilles Current ($3.4 \pm 5.6 \text{ Sv}$) and the DWBC ($-35.2 \pm 9.5 \text{ Sv}$). The large biases in GFDL-ESM4.1 appear to be linked to the overly diffusive and broad Antilles Current and DWBC (Fig. S3).

Overall, the high-resolution MOM6-NWA12 configuration generally shows large improvement in simulating regional ocean circulation and mean conditions compared to the low-resolution GFDL-ESM4.1. Some deficiencies, however, still exist. Potential impacts of these deficiencies on pro-

jected changes, and pathways for future model improvement, will be discussed in Sect. 4.

3.2 Future projections

3.2.1 SST and SSS

We first examine the projected spatial changes in SST and SSS derived from the MOM6-NWA12, comparing the historical period (HIST: 1993–2020) with the late 21st century (L21C: 2073–2100) across four SSP scenarios (SSP-126, SSP-245, SSP-370, and SSP-585). MOM6-NWA12 shows that SST changes in the future exhibit basin-wide warming with discernable end-of-century differences (Fig. 5a–e). The domain-averaged SST warming is lowest in the SSP-126 ($0.52 \text{ }^\circ\text{C}$) simulation and intensifies progressively in SSP-245 ($1.21 \text{ }^\circ\text{C}$), SSP-370 ($1.86 \text{ }^\circ\text{C}$) and SSP-585 ($2.23 \text{ }^\circ\text{C}$) simulations. The SST increase is particularly large in the MAB, the Gulf of Maine, and around the Georges Bank. Temper-

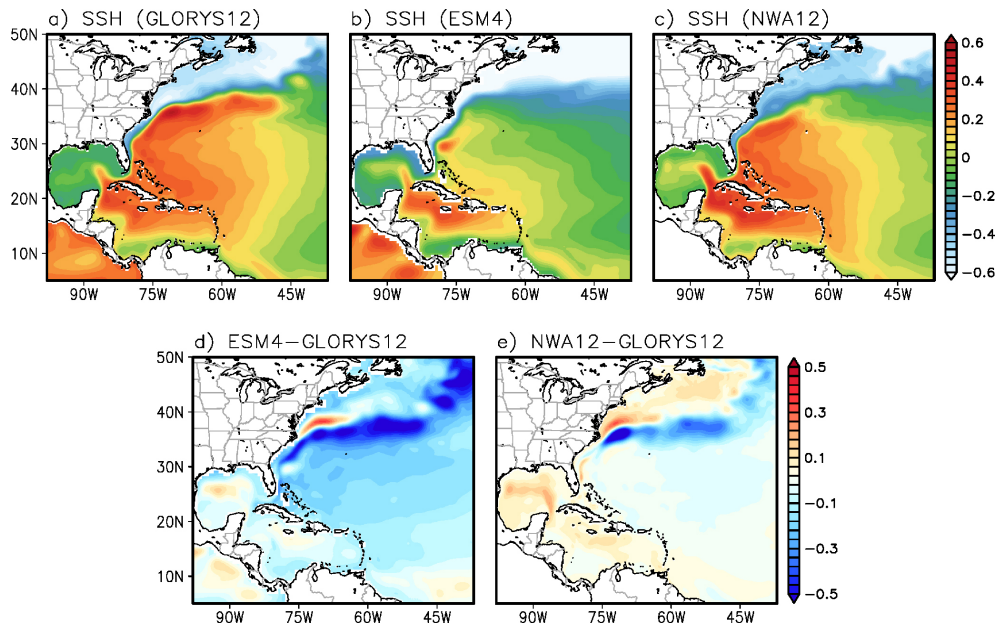


Figure 3. Spatial pattern of the historical (1993–2020) mean sea surface height (SSH, m) in (a) GLORYS12, (b) GFDL-ESM4.1 and (c) MOM6-NWA12. (d) The difference between GFDL-ESM4.1 and GLORYS12. (e) The difference between MOM6-NWA12 and GLORYS12.

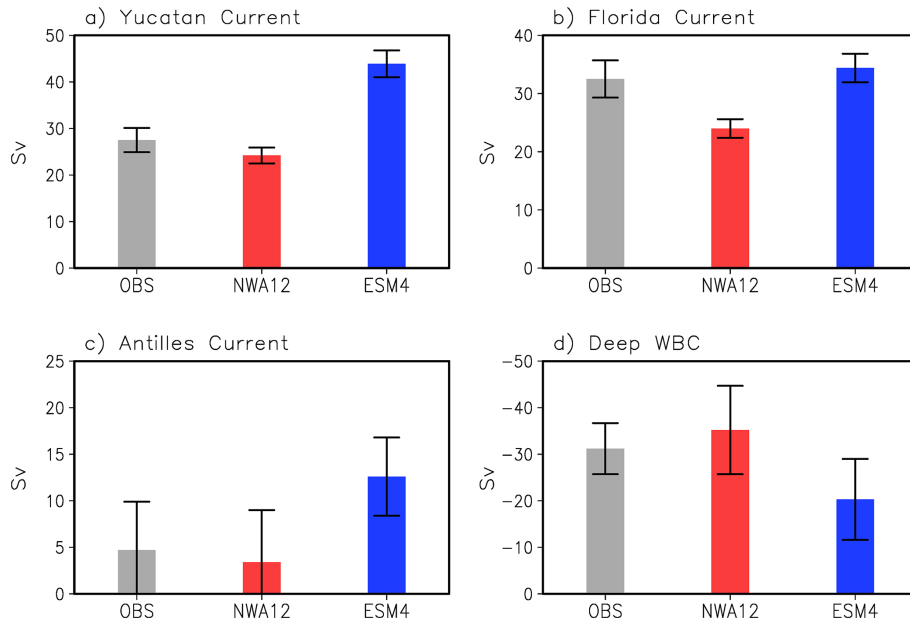


Figure 4. The historical mean (1993–2020) of (a) the Yucatan Channel, (b) Florida Current, (c) Antilles Current, and (d) Deep Western Boundary Current transport derived from observational records (gray bars), MOM6-NWA12 (red bars) and GFDL-ESM4.1 (blue bars). Note that the observational transport records of the Florida Current, Yucatan Current, Antilles Current, and Deep Western Boundary Current (DWBC) are from Volkov et al. (2024), Athié et al. (2020), Meinen et al. (2019) and Zantopp et al. (2017), respectively.

atures are projected to warm by 4 °C in some areas in the SSP-585 scenario (Fig. 5e). Warming in these regions around the MAB and the Gulf of Maine (35–42° N, 75–60° W) is reduced to ~ 3 °C, ~ 2 °C and ~ 1 °C in SSP-370, SSP-245 and SSP-126, respectively (Fig. 5b–d). Mean warming over

the next 30 years (2025–2055), is expected to ~ 1–2 °C with less separation between scenarios (Fig. S4).

Similar to the SST change, the amplitude of the SSS change is sensitive to the SSP scenarios (Fig. 5f–j). The increase in domain-averaged SSS is more pronounced in the higher emission scenarios (0.13 PSU for SSP-126, 0.22 PSU

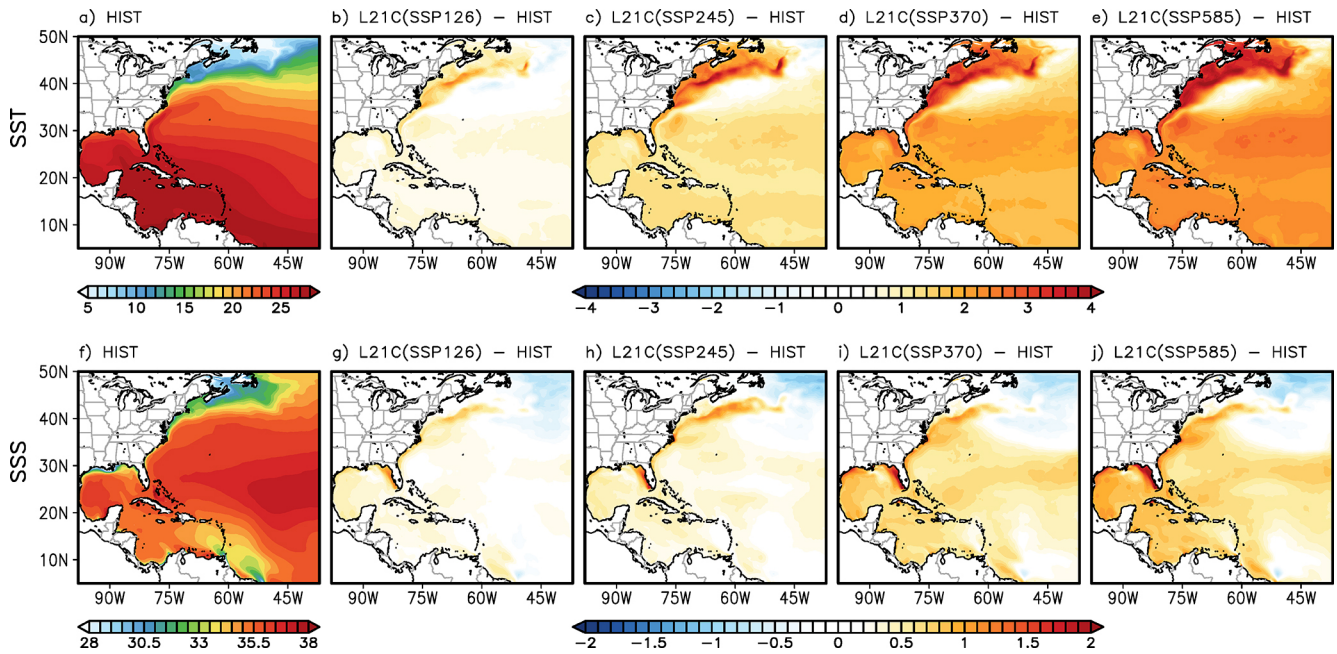


Figure 5. (a) Spatial patterns of sea surface temperature (SST, °C) derived from MOM6-NWA12 during (a) historical period (1993–2020). The differences in SST between the future (2073–2100) and historical periods in the (b) SSP-126, (c) SSP-245, (d) SSP-370 and (e) SSP-585 simulations. (f–j) are the same (a–e) but for sea surface salinity (SSS, PSU).

for SSP-245, 0.41 PSU for SSP-370, and 0.46 PSU for SSP-585). While SSS tends to increase in the subtropical part of the domain, the largest projected SSS increase is along the SAB, the continental slope off the MAB and the West Florida Shelf where the future change intensifies progressively under the high-emission scenarios.

The large increases in SST and SSS on the West Florida Shelf and the SAB appear to be linked to the projected weakening of the Loop Current and Gulf Stream (Fig. 6). Additionally, the weakening of the Gulf Stream leads to a northward shift after its separation from the US East Coast in the late 21st century in all four SSP scenarios (Fig. 6, Sect. 3.2.2), consistent with previous studies (e.g., Saba et al., 2016; Caesar et al., 2018; Bellomo et al., 2021). It appears that the SST increase along the edge of the MAB is linked to the northward shift of the Gulf Stream and the implied warm water intrusion to the Slope Sea (Saba et al., 2016). Warming via this mechanism is fortified by commensurate mean reductions of the advection of cold high-latitude waters from the Labrador Sea as described further in the Discussion section. Interestingly, a narrow region of minimal surface warming is evident immediately south of the historical Gulf Stream path around 35° N, 60° W (Fig. 5e). A similar, but smaller area of minimum surface warming is also evident in the northern GoA, which is largely consistent with previous studies (Liu et al., 2012, 2015). These regions of minimal SST warming appear to be linked to the reduced Gulf Stream or the reduced Loop Current, implying a reduction in ocean heat convergence to these regions (Fig. 6e and i).

While GFDL-ESM4.1 shows the SSP scenario sensitivity for the amplitude of the future SST and SSS changes, the pronounced SST warming identified by MOM6-NWA12 in the Mid-Atlantic Bight (MAB) and Gulf of Maine regions is much reduced in GFDL-ESM4.1 (Fig. 7). This is consistent with the absence of a future northward shift in the Gulf Stream in the coarse resolution GFDL-ESM4.1 (Fig. 8) and prior findings of Saba et al. (2016).

In summary, MOM6-NWA12 projections of SST, SSS, and surface current speed indicate that under all four future scenarios, the Northwestern Atlantic basin becomes significantly warmer, and saltier especially along the US East Coast and the West Florida shelf regions, and the Gulf Stream becomes considerably weaker and shifts northward. The magnitude of projected end-of-century changes, however, varies considerably across scenarios. Most notably, the severity of the impacts projected by the prior worst-case scenario in CMIP6 (i.e., SSP-585) are progressively mitigated by lower emissions scenarios. Differences between scenarios, however, are far smaller in the first half of the century.

3.2.2 WBC transports

As shown in Figs. 6, the entire WBC system, including the North Brazil Current, Caribbean Current, Yucatan Current, Loop Current, Florida Current, and the Gulf Stream, weakens, at least at the surface, consistent with previous future projection studies (e.g., Liu et al., 2012, 2015; Saba et al., 2016; Alexander et al., 2020; Shin and Alexander, 2020;

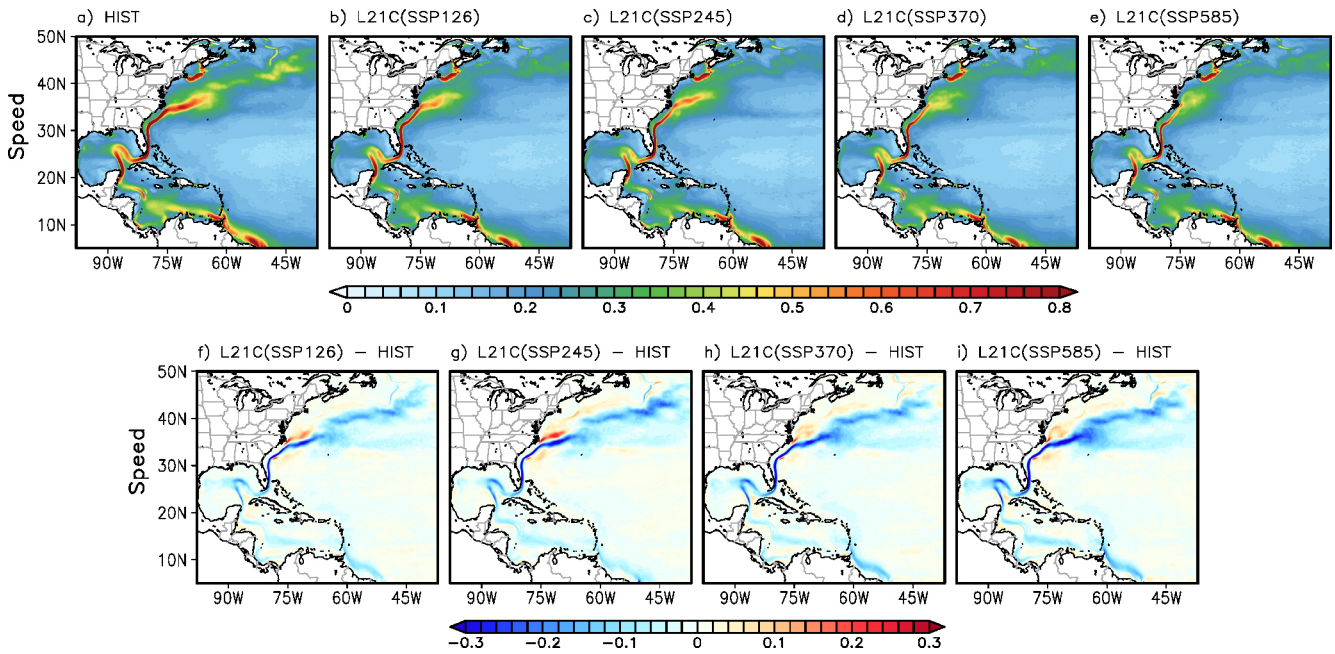


Figure 6. Spatial surface current speed (ms^{-1}) patterns derived from MOM6-NWA12 during (a) the historical (1993–2020) period and future (2073–2100) period in (b) SSP-126, (c) SSP-245, (d) SSP-370 and (e) SSP585 simulations. The difference in surface current speed between the future and historical periods in (f) SSP-126, (g) SSP-245, (h) SSP-370 and (i) SSP585 simulations, respectively.

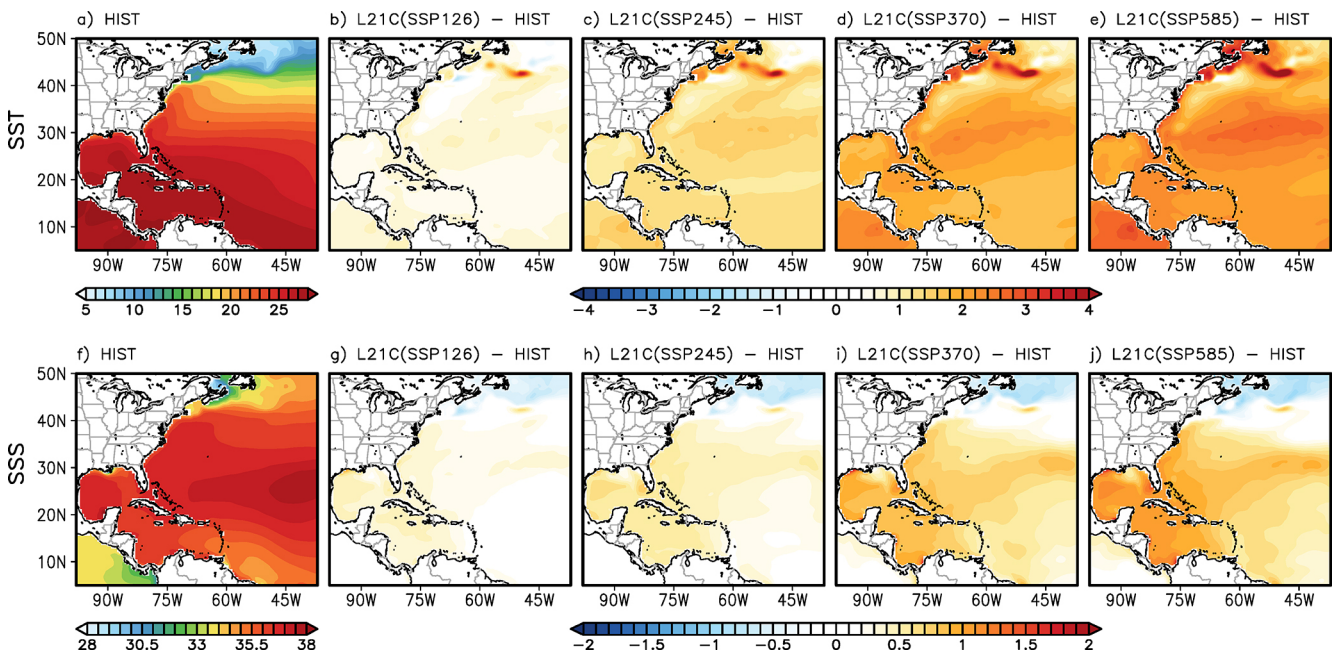


Figure 7. (a) Spatial patterns of sea surface temperature (SST) derived from GFDL-ESM4.1 during the historical period (1993–2020). (b–e) are the differences in SST between the future (2073–2100) and historical (1993–2020) periods in the SSP-126, SSP-245, SSP-370, and SSP-585 simulations, respectively. (f) and (j) are the same (a) and (e) but for the sea surface salinity (SSS).

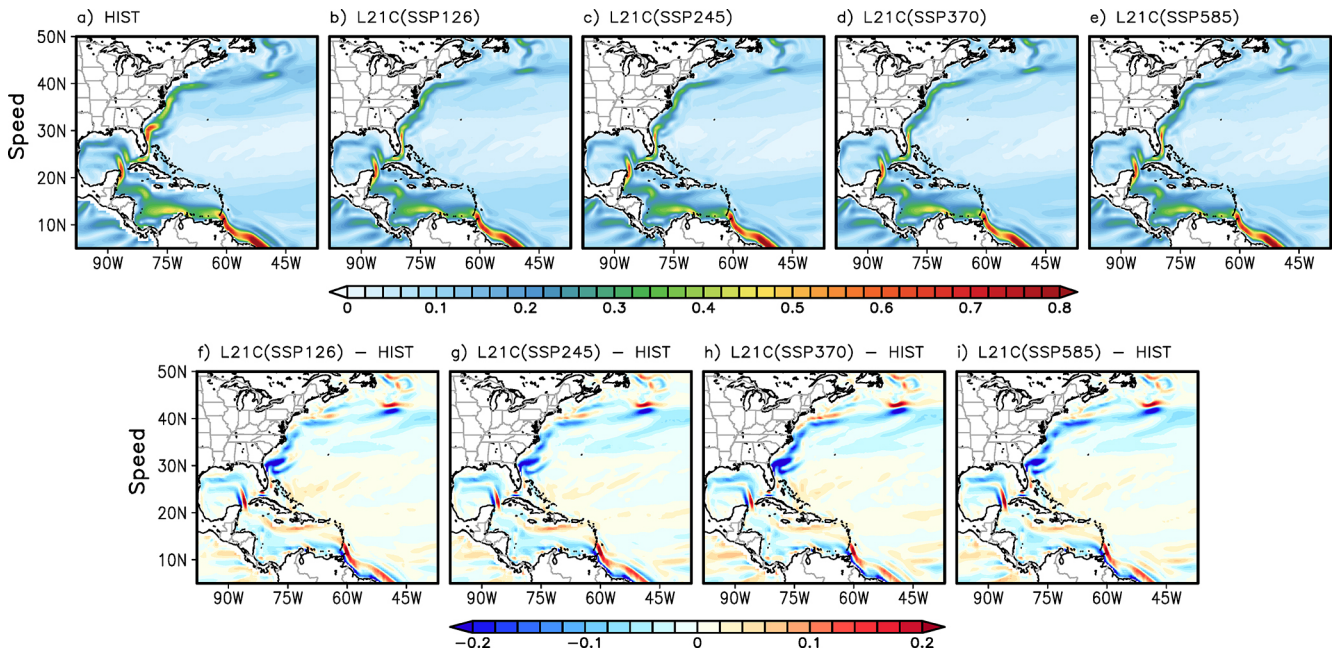


Figure 8. Spatial surface current speed patterns derived from GFDL-ESM4.1 during (a) the historical (1993–2020) period, and future (2073–2100) period in the (b) SSP-126, (c) SSP-245, (d) SSP-370, and (e) SSP-585 simulations. The difference in surface current speed between the future and historical periods in (f) SSP-126, (g) SSP-245, (h) SSP-370, and (i) SSP-585 simulations, respectively.

Beadling et al., 2018; Roberts et al., 2020). The regions of minimal SST warming appear to be linked to the reduced Gulf Stream or the reduced Loop Current, implying a reduction in ocean heat convergence to these regions (Fig. 6e and i). To further explore volume transport by the WBCs system, we examine the temporal changes in the volume transport in the Florida Current, Yucatan Current, Antilles Current, and the Deep Western Boundary Current (DWBC), as shown in Fig. 9.

The Florida Current exhibits a gradual decline throughout the 21st century across all SSP scenarios. The largest decrease in the late 21st century is shown in the SSP-585 scenario (Fig. 9a), from 24.2 ± 1.7 Sv in the historical period to 15.2 ± 3.5 Sv in the late 21st century (37.2% decline) while the smallest decrease in the late 21st century is shown in the SSP-126 scenario (24.3% decline). The intermediate cases more consistent with current CO₂ trajectories also exhibit smaller shifts than the prior worst case. The Yucatan Current shows similar rates of decrease and scenario sensitivity. Under SSP-585, the Yucatan Current transport decreased from 21.0 ± 2.1 Sv in the historical period to 13.2 ± 3.1 Sv in the late 21st century (37.1% decline, Fig. 9b) but end-of-century declines are partially mitigated at intermediate and low emissions cases. The mean transport by the Antilles Current is significantly reduced from 3.4 ± 5.6 Sv in the historical period to -0.72 ± 4.5 Sv in the late 21st century, under SSP-585, with relatively weak variation across scenarios. This suggests that the Antilles Current may disappear (nearly zero mean transport) after around 2080 (Fig. 9c). This weakening

(and the reversal) of the Antilles Current, which is consistent with a previous modeling study (Cai et al., 2024), may play a key role in the subtropical gyre recirculation and the upper-ocean stratification in the SAB. Figure 9d shows that volume transport of the Deep Western Boundary Current (DWBC), which is a vital return flow component of the AMOC from the high latitudes, exhibits the strongest response to anthropogenic warming. Particularly under the SSP-585 scenario, the DWBC transport declines from -35.2 ± 9.5 Sv in the historical period to -20.2 ± 16.0 Sv in the late 21st century (42.7% decline), reflecting a substantial slowdown in the AMOC under SSP-585 (Fig. 10). This slowdown is once again mitigated in part by intermediate and low emissions scenarios.

As was the case for SST, SSS and current speed, the rate of weakening was not very sensitive to the emission scenarios before the 2070s. Similarly, the time series of volume transports in the WBCs system shows a similar rate of decline across all four SSP scenarios until approximately 2070 (Fig. 9). The insensitivity of Northwestern Atlantic WBCs to emission scenarios before 2070s is consistent with the AMOC decline in GFDL-ESM4.1, given that the WBCs are key contributors to the AMOC (Fig. 10). Previous studies (e.g., Weijer et al., 2020; Baker et al., 2023) found that the rate of AMOC weakening derived from most CMIP6 models shows limited sensitivity to emission scenarios prior to around 2070, consistent with GFDL-ESM4.1. It is important to note that the greenhouse gas forcings for the CMIP6 SSP scenarios begin to diverge after the historical period

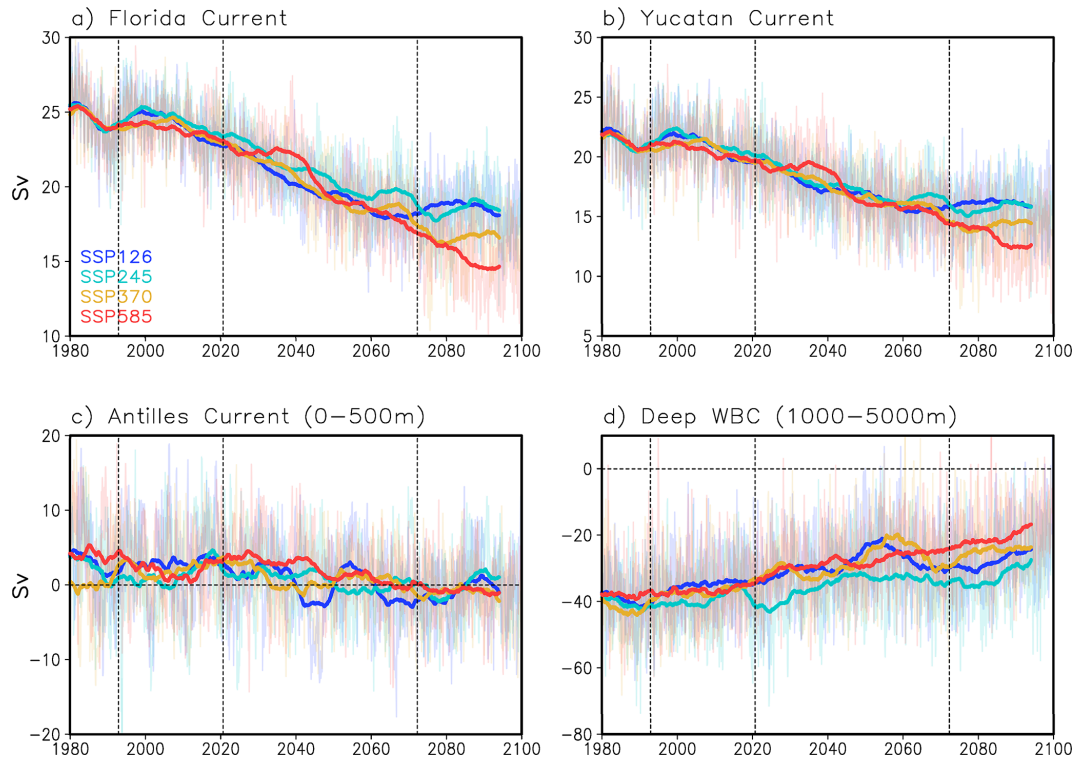


Figure 9. Time series of (a) the Florida Current transport, (b) transport across the Yucatan Channel, (c) Antilles Current transport and (d) Deep Western Boundary Current transport in MOM6-NWA12. The blue, cyan, orange, and red lines are the SSP-126, SSP-245, SSP-370 and SSP-585 simulations, respectively. The bold lines indicate 11-year running means. The vertical dotted lines indicate the historical and future averaging periods.

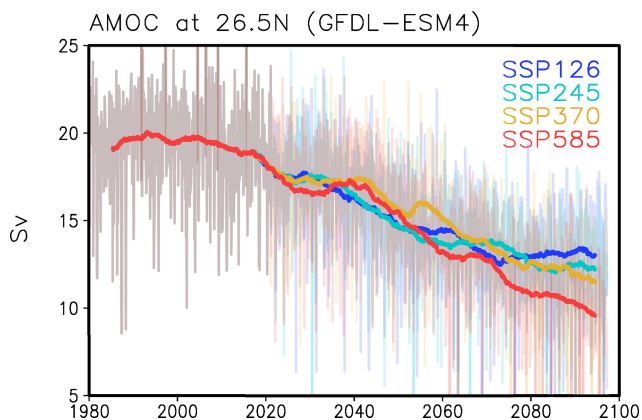


Figure 10. Time series of AMOC in GFDL-ESM4.1. The blue, cyan, orange, and red lines are the SSP-126, SSP-245, SSP-370 and SSP-585 simulations, respectively.

(~ 2014), with separation in their radiative forcing pathways emerging by the mid-21st century. The results that WBC volume transports and AMOC remain relatively insensitive to these diverging emissions scenarios for several decades provides critical evidence for a delayed ocean response to greenhouse gas forcing.

3.2.3 Dynamic SSH

We next explore dynamic SSH and its projected changes under four SSP scenarios (Fig. 11). Substantial changes in both the amplitude and spatial pattern of dynamic SSH are projected in the Northwestern Atlantic. In particular, dynamic SSH increases greatly along the West Florida Shelf (WFS), SAB, MAB, and Georges Bank, and decreases immediately south of the Gulf Stream (after its separation from the US East Coast) under all four SSP scenarios (Fig. 11). Given that these changes are largely confined to the region of WBCs and the southern recirculation (or Worthington) gyre south of the Gulf Stream, the dynamic SSH changes appear to be directly linked to the substantial weakening of the WBC system (e.g., the Loop Current, the Florida Current, and the Gulf Stream) and the implied relaxation of the thermocline slope (i.e., a redistribution of mass) across the WBCs. The projected increases in dynamic SSH along the WFS, SAB, MAB, and the Georges Bank appear to be largely driven by the AMOC weakening (e.g., Yin et al., 2009; Little et al., 2017; Weijer et al., 2020). Note that the dynamic SSH changes in these regions can be also modulated by the future change in the wind-driven gyre circulation, which is not explicitly isolated and evaluated in this study.

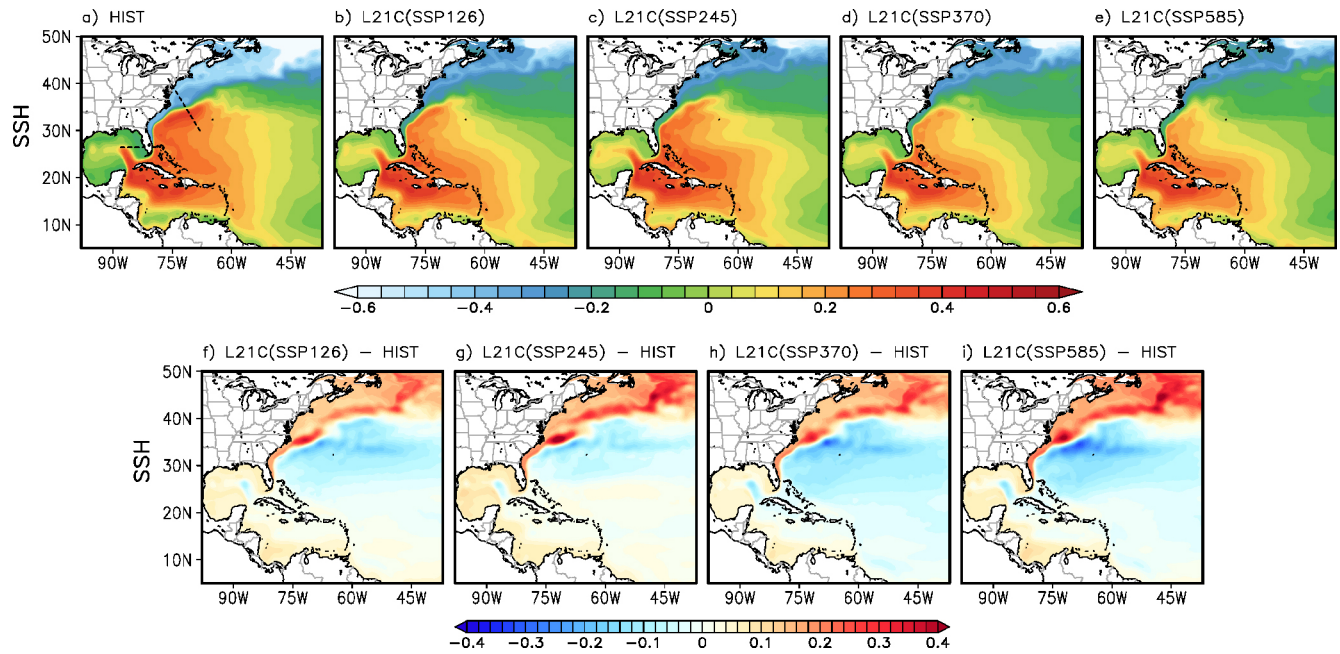


Figure 11. Spatial sea surface height (SSH, m) patterns derived from MOM6-NWA12 during (a) the historical (1993–2020) period, and future (2073–2100) period from (b) SSP-126, (c) SSP-245, (d) SSP-370 and (e) SSP-585 simulations. The difference in SSH between the future and historical periods from (f) SSP-126, (g) SSP-245, (h) SSP-370, and (i) SSP-585 simulations, respectively. The black dotted lines in (a) indicate the locations of vertical cross-section used in Fig. 15–18.

Consistent with MOM6-NWA12, GFDL-ESM4.1 shows an increase in dynamic SSH near the US East Coast and decreases south of the Gulf Stream (after its separation from the US East Coast) in the late 21st century (Fig. 12). An interesting point to note is that MOM6-NWA12 projects a stronger SSH increase in the SAB than in the MAB while GFDL-ESM4.1 projects a stronger SSH increase over the MAB than in the SAB. Consistent with this result, Li et al. (2022) show that the projected SSH derived from a high-resolution Community Earth System Model (CESM) increases more in the SAB than in the MAB, while that derived from a low-resolution CESM increases more in the MAB than in the SAB.

To further explore the future increases in dynamic SSH along the US South and East Coasts, we examine the projected dynamic SSH changes over the continental shelf (i.e., depths < 200 m) for five sub-regions, namely the Northern GoA, WFS, SAB, MAB, and Gulf of Maine, as shown in Fig. 13. The future increase in dynamic SSH is relatively modest in the Northern GoA and WFS, ranging between 5 and 7 cm during the mid- and late-21st century (2041–2100). These increases occur mainly during the mid-21st century (2041–2060), after which there is no significant increase in the dynamic SSH in these shelf regions. Another important feature is that the dynamic SSH increases in the GoA and WFS (Fig. 13a and b) are not sensitive to the emission scenarios considered. Given that the dynamic SSH increase in these regions is mainly driven by the projected weakening

of the AMOC and the associated Loop Current, this result appears to be consistent with the insensitivity in the rate of AMOC's future weakening to the emission scenarios prior to 2070 (Fig. 10).

In contrast to the Northern GoA and WFS, the projected dynamic SSH changes in the US East Coast shelf regions (i.e., SAB, MAB, and Gulf of Maine) are significantly larger, ranging between 10 and 20 cm in the late-21st century. Additionally, unlike the US GoA shelf regions (i.e., Northern GoA and WFS), the increase in dynamic SSH in these regions continues beyond the mid-21st century to the late-21st century, implying that the weakening of the AMOC and the associated WBCs have much tighter control over these regions. A systematic tendency toward greater dynamic SSH changes in higher emissions scenarios also begins to emerge after 2070, though there is still significant variation around this trend (e.g., SSP-370 has a lower local dynamic sea level change than SSP245 despite having higher emissions), presumably due to internal climate variability.

Among the five sub-regions considered, the dynamic SSH change in the SAB is subject to the largest increase. The dynamic SSH in the SAB is projected to increase dramatically after around 2040, reaching close to 20 cm in the late 21st century compared to that in the historical period. This suggests that the SAB is the most sensitive to the projected slowdown of the AMOC and the WBCs in MOM6-NWA12. Specifically, as shown in Fig. 14, a strong negative correlation exists between the Florida Current transport and the

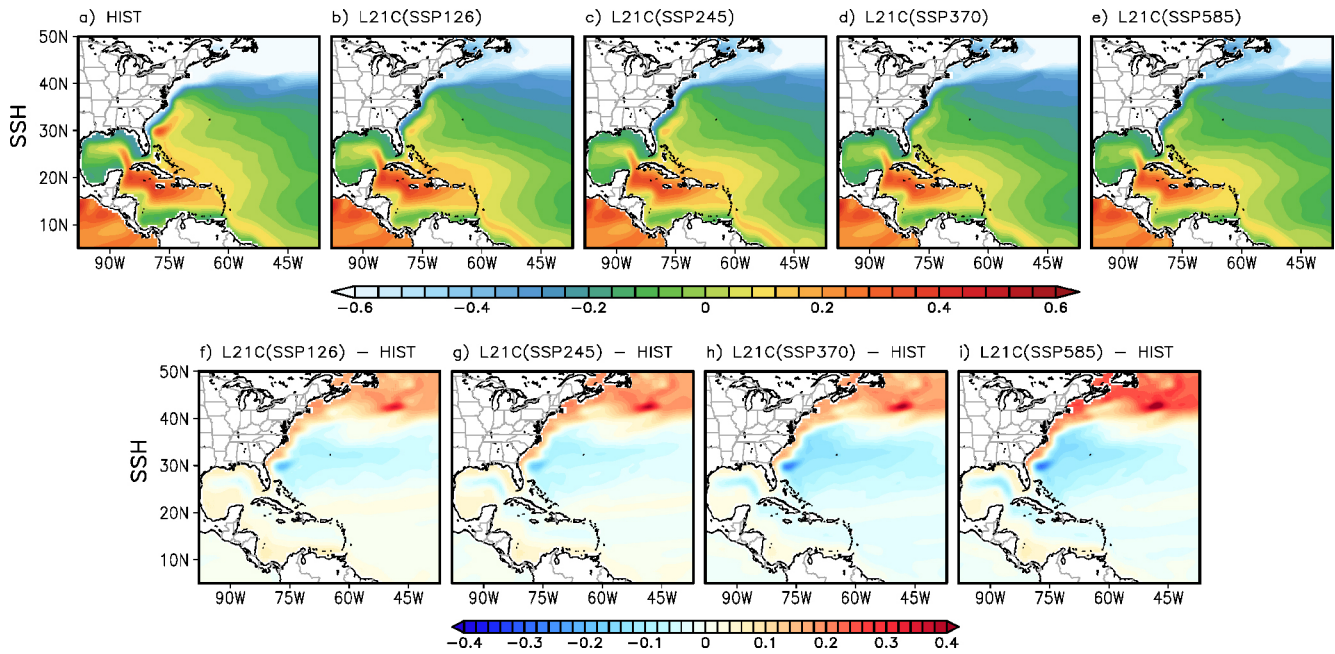


Figure 12. Spatial SSH patterns derived from GFDL-ESM4.1 during (a) the historical (1993–2020) period, and future (2073–2100) period from (b) SSP-126, (c) SSP-245, (d) SSP-370, and (e) SSP-585 simulations, respectively. The difference in SSH between the future and historical periods from (f) SSP-126, (g) SSP-245, (h) SSP-370 and (i) SSP-585 simulations, respectively.

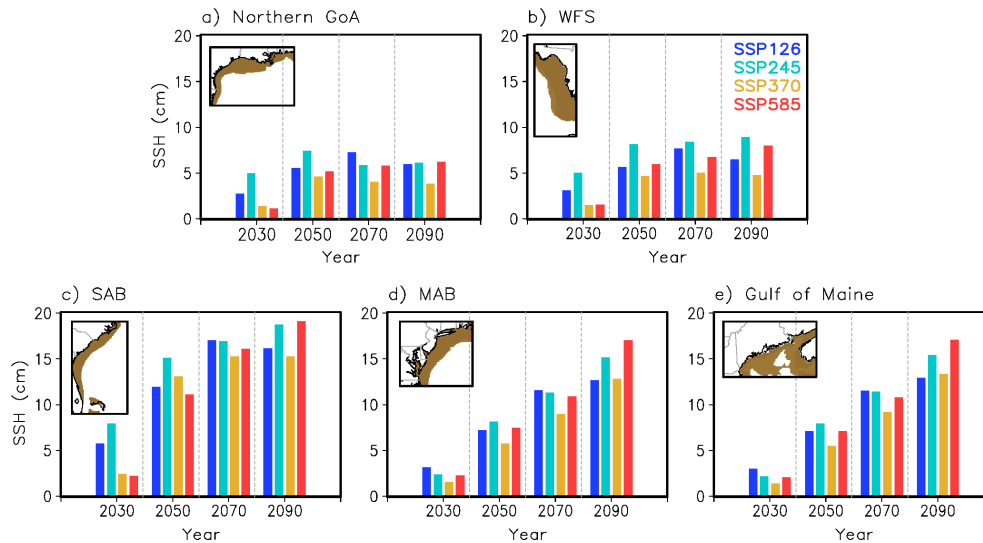


Figure 13. Spatially averaged sea level changes (cm) from historical period (1993–2020) in (a) the northern Gulf of America, (b) West Florida shelf, (c) the South Atlantic Bight, (d) the Middle Atlantic Bight, and (e) the Gulf of Maine under the SSP-126 (blue bars), SSP-245 (cyan bars), SSP-370 (orange bars) and SSP-585 (red bars) simulations. The dynamic sea level changes are spatially averaged over the shelf regions below 200 m depth (brown-colored area in the maps). The years on the *x*-axis represent the center of a 20-year averaging period (e.g., the value for 2030 represents the average from 2021–2040).

SAB dynamic SSH (e.g., Ezer, 2019; Ezer and Atkinson, 2014) indicating that a -1 Sv reduction in the Florida Current transport corresponds to about 1.7 cm of dynamic SSH increase in the SAB. This indicates that the SAB is the future dynamic SSH rise hotspot, potentially posing an increasing

flooding risk in the coastal communities. This appears to be partly due to close proximity of the SAB to the WBC (i.e., Florida Current in this case). In the other subregions, the shelf area is too far away from the WBC (Northern GoA),

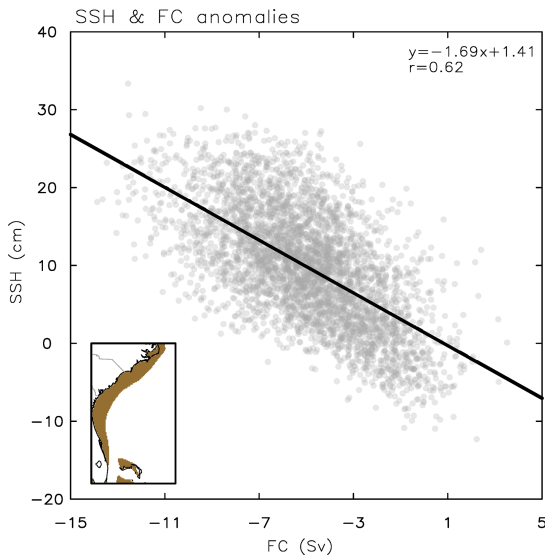


Figure 14. Scatter plot of anomalous Florida Current (FC) transport (Sv) versus dynamic sea level (cm) change along the South Atlantic Bight derived from all four SSP simulations. The dynamic sea level change is spatially averaged over the shelf regions below 200 m (brown-colored area in the map).

too wide (WFS), or mediated by the slope water (MAB and Gulf of Maine).

To better understand the relationship between the SAB dynamic SSH increase and the Gulf Stream weakening, we show the vertical profile of ocean temperature and salinity across 26.5°N during the historical period and their projected changes under the four SSP scenarios (Fig. 15). Figure 15 clearly illustrates a substantial warming and an increase in salinity, mainly along the continental slope and shelf. A distinct decrease in density (i.e., lighter water) emerges on the western side of the Florida Current around 200 m depth (Fig. S5). This localized density reduction reflects a relaxation, or flattening, of the upward-tilted isopycnals along the Florida coast. Consequently, this flattening of the isopycnals weakens the cross-stream horizontal density gradient, thereby reducing northward volume transport in the Florida Straits. Due to reduced bottom Ekman transport and a relaxation, or a flattening, of the upward-tilted isopycnals associated with a weakened Gulf Stream, upwelling decreases along the continental slope and shelf, limiting the supply of cold and relatively fresh subsurface water from underneath the Gulf Stream. This indicates that the warm and salty Gulf Stream water penetrates deeper into the continental slope and shelf region due to the weakening of the Gulf Stream. This baroclinic mass redistribution between the open ocean and the coastal region (from the open ocean to the coast in the upper layers and from the coast to the open ocean deeper down) is also directly responsible for the large projected increase in dynamic SSH across the SAB, which is consistent with the historical analysis of Steinberg et al. (2024). These

future changes in ocean conditions near the coastline are also projected in West Florida. The reduction of the Loop Current leads to an increase in dynamic SSH across West Florida and a significant reduction in the upwelling of cold and relatively fresh subsurface water. This, in turn, results in warm, salty Loop Current water penetrating deeper into the WFS (Fig. 16).

In the MAB ($30\text{--}41^{\circ}\text{N}$, $76\text{--}67^{\circ}\text{W}$), the weakening and shoreward shift of the Gulf Stream in the late 21st century drives an increase in ocean temperature and salinity along the continental slope and shelf (Fig. 17). The maximum SSH anomaly is observed near the core location of the shifted Gulf Stream. Specifically, projected SSH increases on the coastal side of the current while decreasing on the open-ocean side. This differential change results in a reduced cross-stream SSH gradient (slope), consistent with the geostrophic weakening of the flow.

Finally, we emphasize that the dynamical SSH changes driven by changes in ocean currents would occur in addition to the GMSL rise associated with ocean warming and glacial and ice-sheet melt. As described in the methods, MOM6-NWA12 can respond to local density changes driven by local warming and freshening (e.g., Steinberg et al., 2024), even though GMSL rise is not directly reflected in the model simulation due to the Boussinesq approximation. Therefore, to explore the total coastal SSH change (i.e., dynamic SSH changes plus GMSL rise) in the late 21st century, the dynamic SSH changes derived from MOM6-NWA12 are combined with the projected GMSL change. According to the IPCC AR6 report (IPCC, 2023), the projected GMSL rise by the late 21st century relative to the historical period is 0.38 m for SSP-126, 0.47 m for SSP-245, 0.56 m for SSP-370, and 0.64 m for SSP-585, respectively. Specifically, in the SAB under the SSP-585 scenario, the dynamic sea level increase by the late 21st century ($\sim 0.2\text{ m}$) accounts for nearly 25 % of the total sea level increase. This highlights that the SAB could experience extreme and compounding (e.g., high tides and storm surges) coastal flooding risks in the future.

4 Summary and discussion

This study describes and evaluates the dynamically downscaled physics-only MOM6-NWA12 simulations of GFDL-ESM4.1, and then explores future changes of the Northwest Atlantic Ocean under four CMIP6 emission scenarios (SSP-126, SSP-245, SSP-370, and SSP-585). Validation of model outputs against direct ocean observational and reanalysis data shows that the biases in GFDL-ESM4.1 are significantly reduced in MOM6-NWA12, particularly in the spatial SST and SSS patterns, as well as the Gulf Stream's path and volume transport. For instance, while GFDL-ESM4.1 exhibits pronounced warm and high salinity biases along the US East Coast and a northward shift of the Gulf Stream, MOM6-NWA12 simulates improved representation of these key fea-

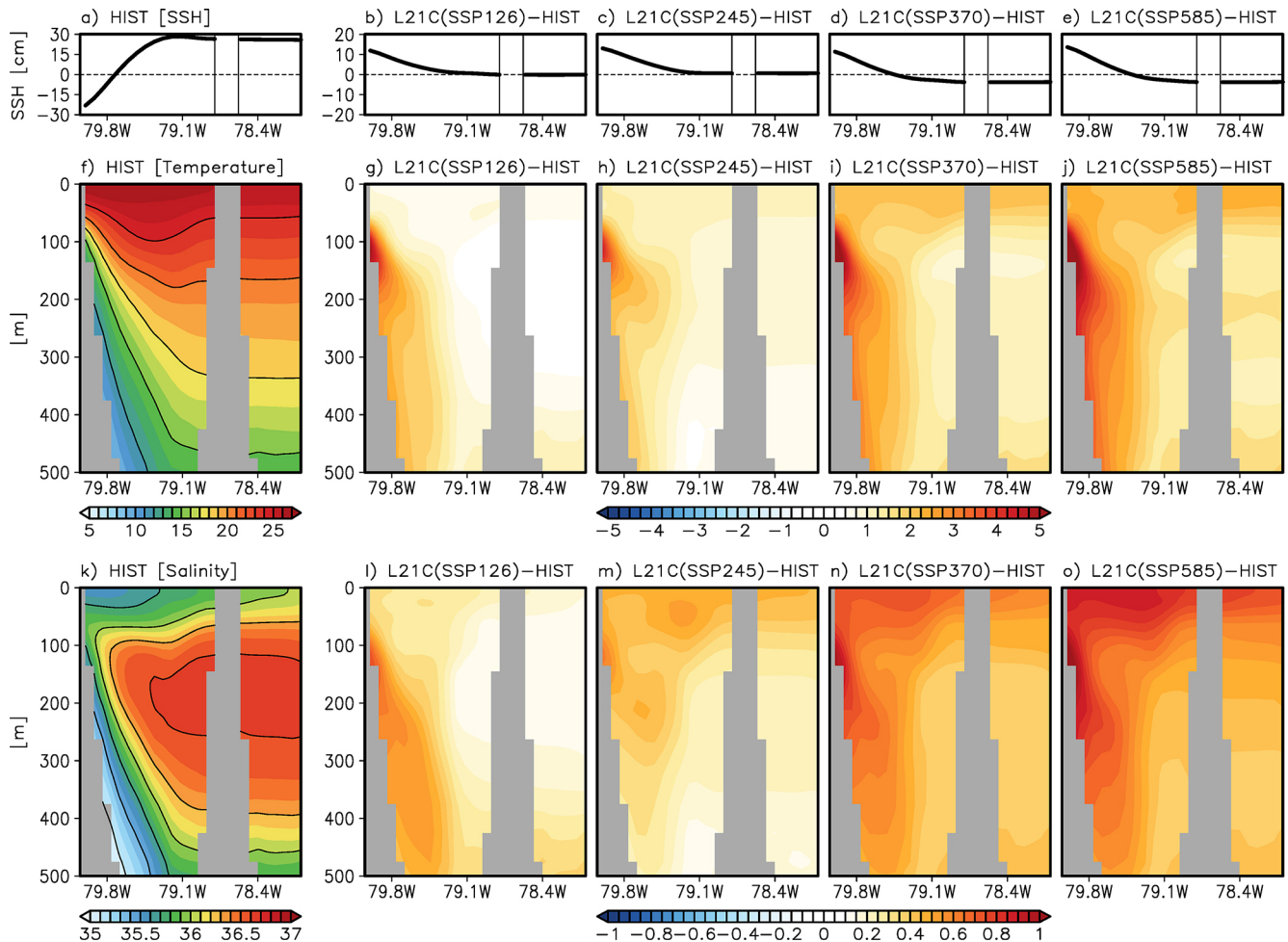


Figure 15. (a) Sea level at the east coast of Florida (26.5° N, 79.7 – 78.0° W) during the historical period. Future change in the sea level at the east coast of Florida from (b) SSP-126, (c) SSP-245, (d) SSP-370, (e) SSP-585, and (c) SSP-585 simulations. (f) The vertical cross-sections of the mean temperature across the east coast of Florida during the historical period. The difference in temperature between the future and historical periods from (g) SSP-126, (h) SSP-245, (i) SSP-370, and (j) SSP-585 simulations, respectively. (k–o) are the same as (f–j) but for salinity.

tures, including a better alignment of the Gulf Stream path with observations. Furthermore, MOM6-NWA12 captures the spatial pattern of SSH much more accurately, as well as the WBCs (i.e., Florida Current, Yucatan Current, Antilles Current, and DWBC).

The projections derived from MOM6-NWA12 show significant changes in SST, SSS and the WBCs under the four SSP scenarios considered. The magnitude of end-of-century changes is strongly scenario-dependent: pronounced SST warming in the MAB and Gulf of Maine, exceeding 4°C in some areas, emerges as a distinct feature of the prior “worst-case” high-emission scenarios (SSP-585), partial mitigation is apparent in intermediate trajectories more consistent with current CO_2 trajectories (SSP-370, SSP-245), and this signal remains modest under low-emission scenarios (SSP-126). The amplified warming and salinification along the US South and East Coasts appears to be linked to a

weakening of the Loop Current and Gulf Stream (e.g., Liu et al., 2012, 2015; Saba et al., 2016) alongside a shoreward and northward shift of the Gulf Stream following its separation from the coast (e.g., Yin et al., 2009; Saba et al., 2016; Bellomo et al., 2021; Li et al., 2022). In addition, as discussed in New et al. (2021), the MAB and the Gulf of Maine are also strongly influenced by the Labrador Current and the Labrador Slope Water (LSLW). The Slope Current in GLORY12 shows the southward Shelf Break Jet in the upper 100 m and the deeper southward flow of LSLW attached to the shelf-slope (Fig. 18a). In contrast, the Slope Current derived in MOM6-NWA12 shows a large bias in its position and strength. More specifically, it is much weaker compared to that in GLORYS12, and is replaced by northward flow in the upper 400 m or so (Fig. 18b). Another core of southward flow appears immediately shoreward of the Gulf Stream in MOM6-NWA12. Since it is positioned away from the con-

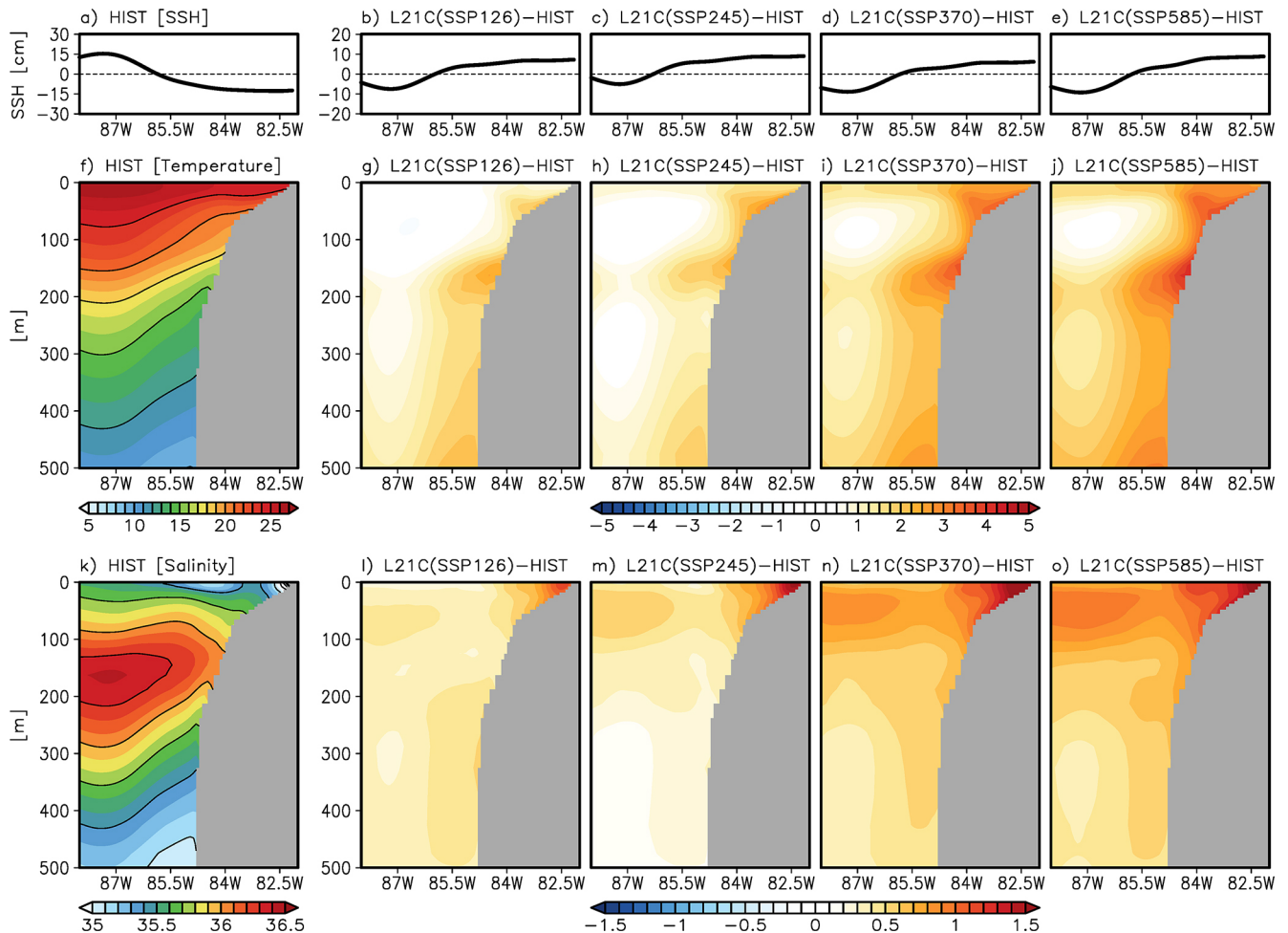


Figure 16. (a) Sea level at West Florida (26.5° N, $88\text{--}81^{\circ}$ W) during the historical period. Future change in the sea level at West Florida from (b) SSP-126, (c) SSP-245, (d) SSP-370, (e) SSP-585, and (e) SSP-585 simulations. (f) The vertical cross-sections of the mean temperature ($^{\circ}$ C) across West Florida during the historical period. The difference in temperature between the future and historical periods from (g) SSP-126, (h) SSP-245, (i) SSP-370, and (j) SSP-585 simulations, respectively. (k–o) are the same as (f–j) but for salinity (PSU).

tinental slope (near 73° W), it is referred to as the northern recirculation flow of the Gulf Stream. In the future scenarios, both the northern recirculation flow and the Slope Current (below 600 m) drastically weaken. The Gulf Stream also weakens and its core shifts shoreward. In the SSP370 and SSP585 scenarios, the Gulf Stream core is positioned along the continental slope. Thus, both the northern recirculation flow and the Slope Current (below 600 m or so) completely disappear in those high emission scenarios. Therefore, despite a large bias in the location and strength of the Slope Current in MOM6-NWA12, we can still conclude that the future warming and saltening in the MAB, shown in Fig. 17, are the result of a compounding effect – a weakening and shoreward shift of the Gulf Stream combined with reduced advection of cold, fresh Labrador Sea waters.

A consistent feature across all projections is the significant deceleration of the surface speed and volume transport of the four WBCs (i.e., Yucatan Current, Florida Current, An-

tilles Current and DWBC), which aligns well with the significant weakening of the AMOC. Reductions in the meridional transports of the four WBCs remain insensitive to emission scenarios until the 2070s, after which they diverge significantly (ranging from $\sim 23\%$ in SSP-126 to $\sim 38\%$ in SSP-585 scenarios).

The projections also suggest that the slowdown of the WBCs leads to an increase in dynamic SSH along the US South and East Coasts, which is largest in the SAB. The increased dynamic SSH in these regions is directly related to the weakening of the WBCs and the associated redistribution of the mass across the WBCs (Minobe et al., 2017). As such, a strong negative correlation exists between the Florida Current transport and the dynamic SSH in the SAB, for example. Further analysis shown in Fig. 15 indicates that the weakening of the Florida Current accompanies a substantial reduction of upwelling of cold and fresh subsurface water to the continental slope and shelf region. The associated decrease

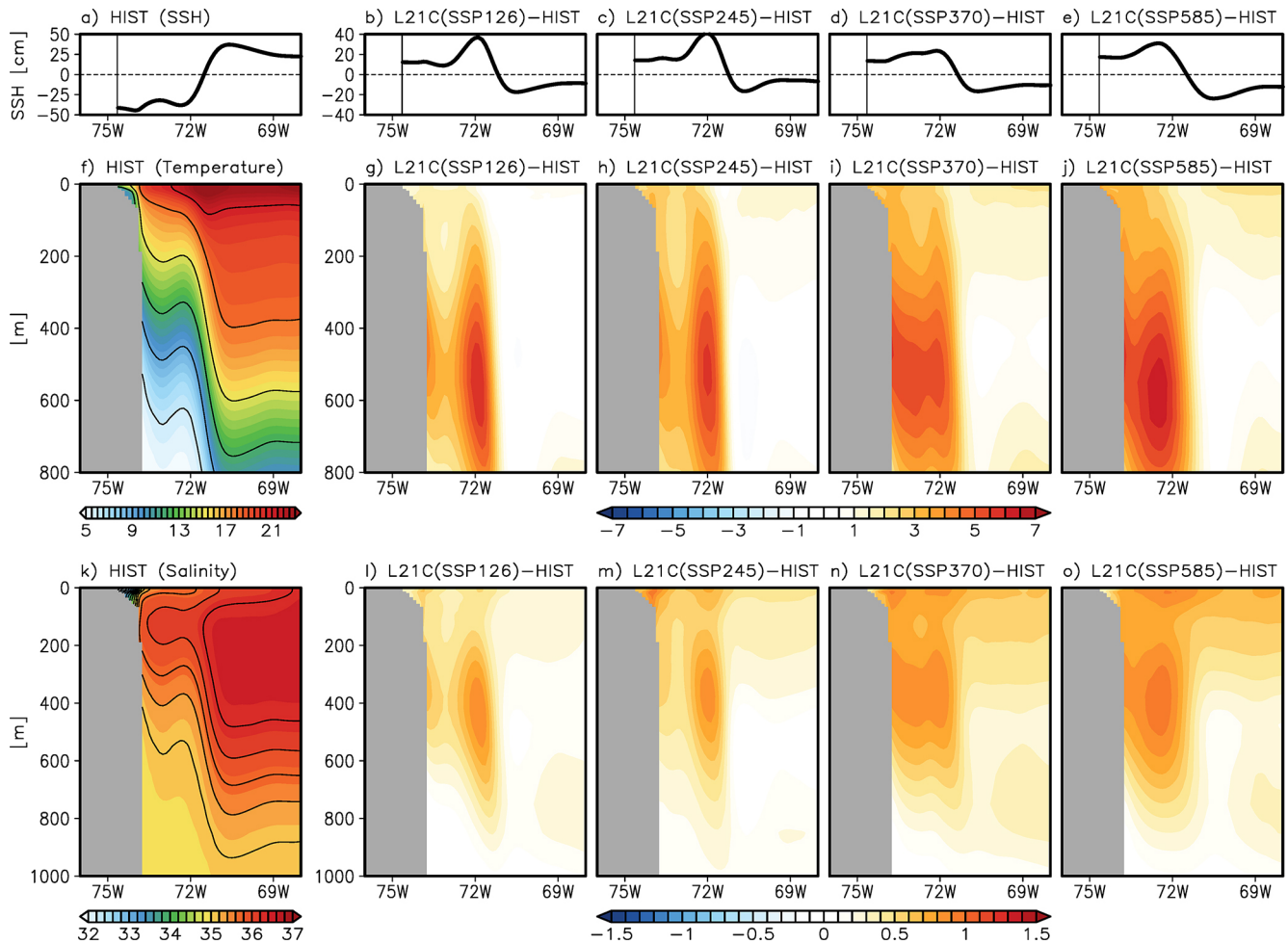


Figure 17. (a) Sea level at the MAB (41–30° N, 76–67° W) during the historical period. Future change in the sea level at the MAB from (b) SSP-126, (c) SSP-245, (d) SSP-370, (e) SSP-585, and (c) SSP-585 simulations. (f) The vertical cross-sections of the mean temperature (°C) across the MAB during the historical period. The difference in temperature between the future and historical periods from (g) SSP-126, (h) SSP-245, (i) SSP-370, and (j) SSP-585 simulations, respectively. (k–o) are the same as (f–j) but for salinity (PSU).

in nutrient supply, implied by the reduced upwelling, has important implications for the marine ecosystems and productivity in the SAB, as the Gulf Stream-induced upwelling represents the main source of nutrients to the SAB outer and mid shelf (e.g., Lee et al., 1991; Gomez et al., 2026).

While this study has mostly focused on describing the future mean changes across scenarios, there are several areas that require further investigation, such as the changes in the seasonal circulation patterns and their impact on the anomalous ocean conditions. This could be relevant, for example, in the MAB where seasonal changes in wind stress drive the annual sea level height variability (e.g., Yang and Chen, 2025). It could also be relevant for the SAB where the seasonal wind stress changes impact coastal temperature and cross-shore interchanges through upwelling (e.g., Castelao, 2011; Yuan et al., 2017). Therefore, further study is needed to explore future changes in the seasonality of WBCs, and their impacts.

Lastly, building on these results derived from physics-only simulations, we plan to couple the physical ocean model with the Carbon, Ocean Biogeochemistry and Lower Trophics (COBALT, Stock et al., 2020, 2025) model to explore future changes in ocean ecosystems in the Northwest Atlantic. Additionally, we will expand the scenario-focused ensemble presented here to include multiple GCMs to fully assess the potential range of the future changes in the Northwest Atlantic.

Code and data availability. The source code for each component of the MOM6-NWA12 model has been archived by Ross et al. (2023) and the GitHub repositories are located at <https://github.com/NOAA-GFDL/CEFI-regional-MOM6> (NOAA-GFDL, 2026). All codes for analyses were performed using the Grid Analysis and Display System (GrADS), which is publicly available from the Center for Ocean–Land–Atmosphere Studies at <https://m.>

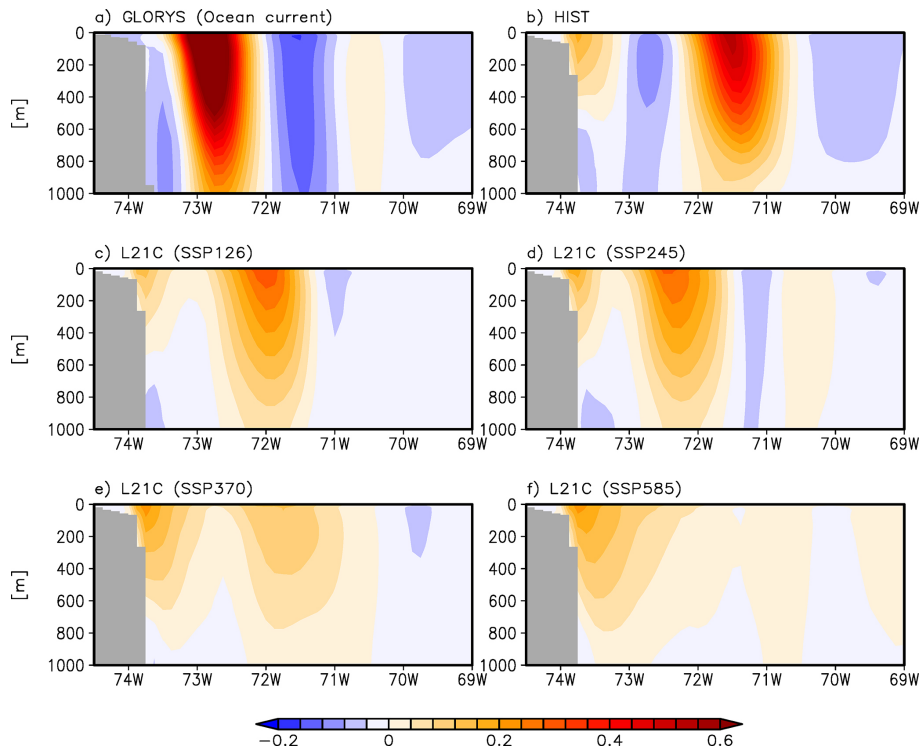


Figure 18. (a) Vertical cross-section of the mean alongshore current across the MAB (41–30° N, 76–67° W) during the historical period (1993–2020) from GLORYS12. (b) Same as (a), but for MOM6-NWA12. (c–f) are the same as (b), but for the future period (2073–2100) from the (c) SSP1-2.6, (d) SSP2-4.5, (e) SSP3-7.0, and (f) SSP5-8.5 simulations, respectively.

monsoondata.org/ (last access: 17 June 2025) and NCL, which is publicly available from the NCAR Command Language (NCL) at <https://www.ncl.ucar.edu/> (last access: 17 June 2026). The GrADS, NCL, and Fortran codes used to perform the analyses can be accessed upon request to Dongmin Kim.

The model outputs derived from the MOM6-NWA12 future projections under four SSP scenarios will be available at CEFI portal soon (https://psl.noaa.gov/cefi_portal/, last access: 17 June 2026). GLORYS12 reanalysis dataset is available at https://data.marine.copernicus.eu/product/GLOBAL_MULTIYEAR_PHY_001_030/description (last access: 17 June 2026). ERA5 reanalysis dataset is available at <https://cds.climate.copernicus.eu/datasets/reanalysis-era5-single-levels> (last access: 17 June 2026). GFDL-ESM4 outputs are freely available at the CMIP6 archive (<https://aims2.llnl.gov/search/cmip6/>, last access: 17 June 2026).

Supplement. The supplement related to this article is available online at <https://doi.org/10.5194/os-22-1987-2026-supplement>.

Author contributions. DK, ACR, SIS and SKL contributed source code for the downscaling system for the regional MOM6. DK, SIS and SKL contributed to preparation of model input files. DK, FAG and SKL contributed to evaluation and interpretation of the model results. DK and SKL prepared the initial draft of the manuscript. All coauthors participated in discussions during vari-

ous stages of the model development and evaluation and read and approved the final version of the manuscript.

Competing interests. At least one of the (co-)authors is a member of the editorial board of *Ocean Science*. The peer-review process was guided by an independent editor, and the authors also have no other competing interests to declare.

Disclaimer. Publisher's note: Copernicus Publications remains neutral with regard to jurisdictional claims made in the text, published maps, institutional affiliations, or any other geographical representation in this paper. The authors bear the ultimate responsibility for providing appropriate place names. Views expressed in the text are those of the authors and do not necessarily reflect the views of the publisher.

Acknowledgements. We would like to sincerely thank Adrian New and an anonymous reviewer for their thorough reviews and thoughtful comments and suggestions, which led to a significant improvement of the paper. We also thank Liz Drenkard for helpful comments and suggestions. This study was supported by the NOAA's Changing Ecosystems, and Fisheries Initiative (CEFI) and the NOAA award Number NA24OARX405C0044-T1-01. This study was also carried out under the auspices of the Cooperative Institute for Marine and Atmospheric Studies (CIMAS) (NOAA co-

operative agreement NA20OAR4320472), the Northern Gulf Institute (NGI) (NOAA cooperative agreement NA21OAR4320190), and supported by NOAA's Oceanic and Atmospheric Research and NOAA's Atlantic Oceanographic and Meteorological Laboratory.

Financial support. This research has been supported by the Cooperative Institute for Marine and Atmospheric Studies, University of Miami (grant no. NA20OAR4320472), the National Oceanic and Atmospheric Administration, Climate Program Office, Changing Ecosystems, and Fisheries Initiative (CEFI) (grant no. NA24OARX405C0044-T1-01), and the Northern Gulf Institute (grant no. NA21OAR4320190).

Review statement. This paper was edited by Anne Marie Treguier and reviewed by Adrian New and one anonymous referee.

References

- Adcroft, A. and Campin, J.-M.: Rescaled height coordinates for accurate representation of free-surface flows in ocean circulation models, *Ocean Model.*, 7, 269–284, <https://doi.org/10.1016/j.ocemod.2003.09.003>, 2004.
- Adcroft, A. and Hallberg, R.: On methods for solving the oceanic equations of motion in generalized vertical coordinates, *Ocean Model.*, 11, 224–233, <https://doi.org/10.1016/j.ocemod.2004.12.007>, 2006.
- Adcroft, A., Anderson, W., Balaji, V., Blanton, C., Bushuk, M., Dufour, C. O., Dunne, J. P., Griffies, S. M., Hallberg, R., Harrison, M. J., Held, I. M., Jansen, M. F., John, J. G., Krasting, J. P., Langenhorst, A. R., Legg, S., Liang, Z., McHugh, C., Radhakrishnan, A., Reichl, B. G., Rosati, T., Samuels, B. L., Shao, A., Stouffer, R., Winton, M., Wittenberg, A. T., Xiang, B., Zadeh, N., and Zhang, R.: The GFDL Global Ocean and Sea Ice Model OM4.0: Model Description and Simulation Features, *J. Adv. Model. Earth Sy.*, 11, 3167–3211, <https://doi.org/10.1029/2019MS001726>, 2019.
- Alexander, M. A. and Scott, J. D.: The Role of Ekman Ocean Heat Transport in the Northern Hemisphere Response to ENSO, *J. Climate*, 21, 5688–5707, <https://doi.org/10.1175/2008JCLI2382.1>, 2008.
- Alexander, M. A., Shin, S., Scott, J. D., Curchitser, E., and Stock, C.: The Response of the Northwest Atlantic Ocean to Climate Change, *J. Climate*, 33, 405–428, <https://doi.org/10.1175/JCLI-D-19-0117.1>, 2020.
- Alfieri, L., Lorini, V., Hirpa, F. A., Harrigan, S., Zsoter, E., Prudhomme, C., and Salamon, P.: A Global Streamflow Reanalysis for 1980–2018, *J. Hydrol.*, 6, 100049, <https://doi.org/10.1016/j.hydroa.2019.100049>, 2020.
- Athié, G., Sheinbaum, J., Leben, R., Ochoa, J., Shannon, M. R., and Candela, J.: Interannual variability in the Yucatan Channel flow, *Geophys. Res. Lett.*, 42, 1496–1503, <https://doi.org/10.1002/2014GL062674>, 2015.
- Athié, G., Sheinbaum, J., Candela, J., Ochoa, J., Pérez-Brunius, P., and Romero-Arteaga, A.: Seasonal Variability of the Transport through the Yucatan Channel from Observations, *J. Phys. Oceanogr.*, 50, 343–360, <https://doi.org/10.1175/JPO-D-18-0269.1>, 2020.
- Baker, J. A., Bell, M. J., Jackson, L. C., Renshaw, R., Vallis, G. K., Watson, A. J., and Wood, R. A.: Overturning pathways control AMOC weakening in CMIP6 models, *Geophys. Res. Lett.*, 50, e2023GL103381, <https://doi.org/10.1029/2023GL103381>, 2023.
- Beadling, R. L., Russell, J. L., Stouffer, R. J., and Goodman, P. J.: Evaluation of subtropical North Atlantic Ocean circulation in CMIP5 models against the observational array at 26.5° N and its changes under continued warming, *J. Climate*, 31, 9697–9718, <https://doi.org/10.1175/jcli-d-17-0845.1>, 2018.
- Bell, R. J., Richardson, D. E., Hare, J. A., Lynch, P. D., and Fratantoni, P. S.: Disentangling the effects of climate, abundance, and size on the distribution of marine fish: an example based on four stocks from the Northeast US shelf, *ICES J. Mar. Sci.*, 72, 1311–1322, <https://doi.org/10.1093/icesjms/fsu217>, 2015.
- Bellomo, K., Angeloni, M., Corti, S., and Hardenberg, J.: Future climate change shaped by inter-model differences in Atlantic meridional overturning circulation response, *Nat. Commun.*, 12, 3659, <https://doi.org/10.1038/s41467-021-24015-w>, 2021.
- Caesar, L., Rahmstorf, S., Robinson, Feulner, G., and Saba, V.: Observed fingerprint of a weakening Atlantic Ocean overturning circulation, *Nature*, 556, 191–196, <https://doi.org/10.1038/s41586-018-0006-5>, 2018.
- Cai, J., Yang, H., Chen, Z., and Wu, L.: The disappearing Antilles Current dominates the weakening meridional heat transport in the North Atlantic Ocean under global warming, *Environ. Res. Lett.*, 19, 044049, <https://doi.org/10.1088/1748-9326/ad3567>, 2024.
- Castelao, R.: Intrusions of Gulf Stream waters onto the South Atlantic Bight shelf, *J. Geophys. Res.-Oceans*, 116, C10011, <https://doi.org/10.1029/2011JC007178>, 2011.
- Chassignet, E. and Marshall, D.: Gulf Stream separation in numerical ocean models, in: *Ocean Modeling in an Eddy Regime*, Geoph. Monog. Series 177, Wiley, <https://doi.org/10.1029/GM177>, 2008.
- Cheng, C. S., Li, G., Li, Q., Auld, H., and Fu, C.: Possible Impacts of Climate Change on Wind Gusts under Downscaled Future Climate Conditions over Ontario, Canada, *J. Climate*, 25, 3390–3408, <https://doi.org/10.1175/JCLI-D-11-00198.1>, 2012.
- Domingues, R., Goni, G., Baringer, M., and Volkov, D.: What caused the accelerated sea level changes along the U. S. East Coast during 2010–2015?, *Geophys. Res. Lett.*, 45, 13367–13376, <https://doi.org/10.1029/2018GL081183>, 2018.
- Dong, S., Baringer, M., and Goni, G.: Slowdown of the Gulf Stream during 1993–2016, *Sci. Rep.*, 9, 6672, <https://doi.org/10.1038/s41598-019-42820-8>, 2019.
- Drenkard, E. J., Stock, C., Ross, A. C., Dixon, K. W., Adcroft, A., Alexander, M., Balaji, V., Bograd, S. J., Butenschön, M., Cheng, W., Curchitser, E., Lorenzo, E. D., Dussin, R., Haynie, A. C., Harrison, M., Hermann, A., Hollowed, A., Holsman, K., Holt, J., Jacox, M. G., Jang, C. J., Kearney, K. A., Muhling, B. A., Buil, M. P., Saba, V., Sandø, A. B., Tommasi, D., and Wang, M.: Next-generation regional ocean projections for living marine resource management in a changing climate, *ICES J. Mar. Sci.*, 78, 1969–1987, <https://doi.org/10.1093/icesjms/fsab100>, 2021.
- Dunne, J. P., Horowitz, L. W., Adcroft, A. J., Ginoux, P., Held, I. M., John, J. G., Krasting, J. P., Malyshev, S.,

- Naik, V., Paulot, F., Shevliakova, E., Stock, C. A., Zadeh, N., Balaji, V., Blanton, C., Dunne, K. A., Dupuis, C., Durachta, J., Dussin, R., Gauthier, P. P. G., Griffies, S. M., Guo, H., Hallberg, R. W., Harrison, M., He, J., Hurlin, W., McHugh, C., Menzel, R., Milly, P. C. D., Nikonov, S., Paynter, D. J., Ploshay, J., Radhakrishnan, A., Rand, K., Reichl, B. G., Robinson, T., Schwarzkopf, D. M., Sentman, L. T., Underwood, S., Vahlenkamp, H., and Winton, M.: The GFDL Earth System Model Version 4.1 (GFDL-ESM 4.1): Overall coupled model description and simulation characteristic, *J. Adv. Model. Earth Sy.*, 12, e2019MS002015, <https://doi.org/10.1029/2019MS002015>, 2020.
- Ezer, T.: Detecting changes in the transport of the Gulf Stream and the Atlantic overturning circulation from coastal sea level data: The extreme decline in 2009–2010 and estimated variations for 1935–2012, *Global Planet. Change*, 129, 23–36, <https://doi.org/10.1016/j.gloplacha.2015.03.002>, 2015.
- Ezer, T.: Regional differences in sea level rise between the Mid-Atlantic Bight and the South Atlantic Bight: Is the Gulf Stream to blame?, *Earths Future*, 7, 771–783, <https://doi.org/10.1029/2019EF001174>, 2019.
- Ezer, T. and Atkinson, L. P.: Accelerated flooding along the US East Coast: On the impact of sea-level rise, tides, storms, the Gulf Stream, and the North Atlantic Oscillations, *Earths Future*, 2, <https://doi.org/10.1002/2014EF000252>, 2014.
- Ezer, T., Atkinson, L. P., Corlett, W. B., and Blanco, J. L.: Gulf Stream's induced sea level rise and variability along the US mid-Atlantic coast, *J. Geophys. Res.-Oceans*, 118, 685–697, <https://doi.org/10.1002/jgrc.20091>, 2013.
- Friedrichs, M. A. M., St-Laurent, P., Xiao, Y., Hofmann, E., Hyde, K., Mannino, A., Najjar, R. G., Narváez, D. A., Signorini, S. R., Tian, H., Wilkin, J., Yao, Y., and Xue, J.: Ocean circulation causes strong variability in the Mid-Atlantic Bight nitrogen budget, *J. Geophys. Res.-Oceans*, 124, 113–134, <https://doi.org/10.1029/2018JC014424>, 2019.
- Goddard, P. B., Yin, J., Griffies, S. M., and Zhang, S.: An extreme event of sea-level rise along the Northeast coast of North America in 2009–2010, *Nat. Commun.*, 6, <https://doi.org/10.1038/ncomms7346>, 2015.
- Gomez, F. A., Lee, S. K., Hernandez, F. J., Chiaverano, L. M., Muller-Karger, F. E., Liu, Y., and Lamkin, J. T.: ENSO-induced co-variability of Salinity, Plankton Biomass and Coastal Currents in the Northern Gulf of Mexico, *Sci. Rep.*, 9, 178, <https://doi.org/10.1038/s41598-018-36655-y>, 2019.
- Gomez, F. A., Wanninkhof, R., Barbero, L., Lee, S.-K., and Hernandez Jr., F. J.: Seasonal patterns of surface inorganic carbon system variables in the Gulf of Mexico inferred from a regional high-resolution ocean biogeochemical model, *Biogeosciences*, 17, 1685–1700, <https://doi.org/10.5194/bg-17-1685-2020>, 2020.
- Gomez, F. A., Lee, S.-K., Stock, C. A., Ross, A. C., Resplandy, L., Siedlecki, S. A., Tagklis, F., and Salisbury, J. E.: RC4USCoast: a river chemistry dataset for regional ocean model applications in the US East Coast, Gulf of Mexico, and US West Coast, *Earth Syst. Sci. Data*, 15, 2223–2234, <https://doi.org/10.5194/essd-15-2223-2023>, 2023.
- Gomez, F. A., Wanninkhof, R., Barbero, L., and Lee, S.-K.: Mississippi River Chemistry Impacts on the Interannual Variability of Aragonite Saturation State in the Northern Gulf of Mexico, *J. Geophys. Res.-Oceans*, 129, e2023JC020436, <https://doi.org/10.1029/2023JC020436>, 2024.
- Gomez, F. A., Ross, A. C., Lee, S.-K., Volkov, D., Kim, D., John, J. G., and Stock, C. A.: Wind control of the interannual ocean-biogeochemical variability in the South Atlantic Bight, *J. Geophys. Res.-Oceans*, 131, e2025JC023322, <https://doi.org/10.1029/2025JC023322>, 2026.
- Greatbatch, R. J.: A note on the representation of steric sea level in models that conserve volume rather than mass, *J. Geophys. Res.-Oceans*, 99, 12767–12771, <https://doi.org/10.1029/94JC00847>, 1994.
- Griffies, S. M. and Greatbatch, R. J.: Physical processes that impact the evolution of global mean sea level in ocean climate models, *Ocean Model.*, 51, 37–72, 2012.
- Griffies, S. M., Yin, J., Durack, P. J., Goddard, P., Bates, S. C., Behrens, E., Bentsen, M., Bi, D., Biastoch, A., Böning, C., Bozec, A., Chassignet, E., Danabasoglu, G., Danilov, S., Domingues, C. M., Drange, H., Farneti, R., Fernandez, E., Greatbatch, R. J., Holland, D. M., Ilicak, M., Large, W. G., Lorbacher, K., Lu, J., Marsland, S. J., Mishra, A., Nurser, A. J. G., Salas y Mélia, D., Palter, J. B., Samuels, B. L., Schröter, Schwarzkopf, F. U., Sidorenko, D., Treguier, A.-M., Tseng, Y. H., Tsujino, H., Uotila, P., Valcke, S., Voldoire, A., Wang, Q., Winton, M., and Zhang, X.: An assessment of global and regional sea level for years 1993–2007 in a suite of interannual CORE-II simulations, *Ocean Model.*, 78, 35–89, <https://doi.org/10.1016/j.ocemod.2014.03.004>, 2014.
- Hameed, S. C., Wolfe, L. P., and Chi, L.: Impact of the Atlantic Meridional Mode on Gulf Stream North Wall Position, *J. Climate*, 31, 8875–8894, <https://doi.org/10.1175/JCLI-D-18-0098.1>, 2018.
- Hersbach, H., Bell, B., Berrisford, P., Hirahara, S., Horányi, A., Muñoz-Sabater, J., Nicolas, J., Peubey, C., Radu, R., Schepers, D., Simmons, A., Soci, C., Abdalla, S., Abellan, X., Balsamo, G., Bechtold, P., Biavati, G., Bidlot, J., Bonavita, M., De Chiara, G., Dahlgren, P., Dee, D., Diamantakis, M., Dragani, R., Flemming, J., Forbes, R., Fuentes, M., Geer, A., Haimberger, L., Healy, S., Hogan, R. J., Hólm, E., Janisková, M., Keeley, S., Laloyaux, P., Lopez, P., Lupu, C., Radnoti, G., de Rosnay, P., Rozum, I., Vamborg, F., Villaume, S., and Thépaut, J.-N.: The ERA5 Global Reanalysis, *Q. J. Roy. Meteor. Soc.*, 146, 1999–2049, <https://doi.org/10.1002/qj.3803>, 2020.
- Huang, L., Volkov, D. L., Dong, S., and Schmid, C.: On the rapid warming in the subtropical North Atlantic in 2011–2021, *Geophys. Res. Lett.*, 52, e2025GL116280, <https://doi.org/10.1029/2025GL116280>, 2025.
- IPCC – Intergovernmental Panel On Climate Change: Climate Change 2021 – The Physical Science Basis: Working Group I Contribution to the Sixth Assessment Report of the Intergovernmental Panel on Climate Change, Cambridge University Press, <https://doi.org/10.1017/9781009157896>, 2023.
- Jeong, D. I. and Sushama, L.: Projected Changes to Mean and Extreme Surface Wind Speeds for North America Based on Regional Climate Model Simulations, *Atmosphere*, 10, 497, <https://doi.org/10.3390/atmos10090497>, 2019.
- Karnauskas, M., Schirripa, M. J., Kelble, C. K., Cook, G. S., and Craig, J. K.: Ecosystem status report for the Gulf of Mexico, NOAA Technical Memorandum NMFS-SEFSC-653,

- <https://repository.library.noaa.gov/view/noaa/4575> (last access: 17 June 2026), 2013.
- Karnauskas, M., Schirripa, M. J., Craig, K., Cook, G., Kelble, C., Agar, J., Black, B., Enfield, D., Lindo-Atichati, D., Muhling, B., Purcell, K., Richards, P., and Wang, C. Evidence of climate-driven ecosystem reorganization in the Gulf of Mexico, *Glob. Change Biol.*, 21, 2554–2568, 2015.
- Koul, V., Ross, A. C., Stock, C., Zhang, L., Delworth, T., and Wittenberg, A.: A predicted pause in the rapid warming of the Northwest Atlantic Shelf in the coming decade, *Geophys. Res. Lett.*, 51, e2024GL110946, <https://doi.org/10.1029/2024GL110946>, 2024.
- Lee, T. N., Yoder, J. A., and Atkinson, L. P.: Gulf Stream frontal eddy influence on productivity of the 857 southeast US Continental Shelf, *J. Geophys. Res.-Oceans*, 96, 191–205, <https://doi.org/10.1029/91jc02450>, 1991.
- Lellouche, J., Greiner, E., Bourdallé-Badie, R., Garric, G., Melet, A., Drévilion, M., Bricaud, C., Hamon, M., Le Galloudec, O., Regnier, C., Candela, T., Testut, C., Gasparin, F., Ruggiero, G., Benkiran, M., Drillet, Y., and Le Traon, P.: The Copernicus Global 1/12 Oceanic and Sea Ice GLORYS12 Reanalysis, *Front. Earth Sci.*, 9, 698876, <https://doi.org/10.3389/feart.2021.698876>, 2021.
- Levermann, A., Griesel, A., Hofmann, M., Montoya, M., and Rahmstorf, S.: Dynamic sea level changes following changes in the thermohaline circulation, *Clim. Dynam.*, 24, 347–354, <https://doi.org/10.1007/s00382-004-0505-y>, 2005.
- Li, D., Chang, P., Yeager, S. G., Danabasoglu, G., Castruccio, F. S., Small, Wang, H., Zhang, Q., and Gopal, A.: The impact of horizontal resolution on projected sea-level rise along US east continental shelf with the community earth system model, *J. Adv. Model. Earth Sy.*, 14, e2021MS002868, 2022.
- Lin, S. J.: A “vertically Lagrangian” finite-volume dynamical core for global models, *Mon. Weather Rev.*, 132, 2293–2307, 2004.
- Little, C. M., Piecuch, C. G., and Ponte, R. M.: On the relationship between the meridional overturning circulation, alongshore wind stress, and United States East Coast sea level in the Community Earth System Model Large Ensemble, *J. Geophys. Res.-Oceans*, 122, 4554–4568, <https://doi.org/10.1002/2017JC012713>, 2017.
- Little, C. M., Hu, A., Hughes, C. W., McCarthy, G. D., Piecuch, C. G., Ponte, R. M., and Thomas, M. D.: The Relationship between U. S. East Coast sea level and the Atlantic Meridional Overturning Circulation: A review, *J. Geophys. Res.-Oceans*, 124, 6435–6458, <https://doi.org/10.1029/2019JC015152>, 2019.
- Liu, Y., Lee, S.-K., Muhling, B. A., Lamkin, J. T., and Enfield, D. B.: Significant reduction of the Loop Current in the 21st century and its impact on the Gulf of Mexico, *J. Geophys. Res.-Oceans*, 117, C05039, <https://doi.org/10.1029/2011JC007555>, 2012.
- Liu, Y., Lee, S.-K., Enfield, D. B., Muhling, B. A., Lamkin, J. T., Muller-Karger, F. E., and Roffer, M. A.: Potential impact of climate change on the Intra-Americas Sea: Part-1. A dynamic downscaling of the CMIP5 model projections, *J. Marine Syst.*, 148, 56–69, <https://doi.org/10.1016/j.jmarsys.2015.01.007>, 2015.
- McCarthy, G. D., Smeed, D. A., Johns, W. E., Frajka-Williams, E., Moat, B. I., Rayner, D., Baringer, M. O., Meinen, C. S., Collins, J., and Bryden, H. L.: Measuring the Atlantic Meridional Overturning Circulation at 26° N, *Prog. Oceanogr.*, 130, 91–111, <https://doi.org/10.1016/j.pocan.2014.10.006>, 2015.
- Meehl, G. A., Senior, C. A., Eyring, V., Flato, G., Lamarque, J.-F., Stouffer, R. J., Taylor, K. E., and Schlund, M.: Context for interpreting equilibrium climate sensitivity and transient climate response from the CMIP6 Earth system models, *Sci. Adv.*, 6, eaba1981, <https://doi.org/10.1126/sciadv.aba1981>, 2020.
- Meinen, C. S., Johns, W. E., Moat, B. I., Smith, R. H., Johns, E. M., Rayner, D., Frajka-Williams, E., Garcia, R. F., and Garzoli, S. L.: Structure and variability of the Antilles Current at 26.5° N, *J. Geophys. Res.-Oceans*, 124, 3700–3723, <https://doi.org/10.1029/2018JC014836>, 2019.
- Minobe, S., Terada, M., Qiu, B., and Schneider, N.: Western boundary sea level: A theory, rule of thumb, and application to climate models, *J. Phys. Oceanogr.*, 47, 957–977, <https://doi.org/10.1175/JPO-D-16-0144.1>, 2017.
- Müller, O. V., McGuire, P. C., Vidale, P. L., and Hawkins, E.: River flow in the near future: a global perspective in the context of a high-emission climate change scenario, *Hydrol. Earth Syst. Sci.*, 28, 2179–2201, <https://doi.org/10.5194/hess-28-2179-2024>, 2024.
- Muller-Karger, F. E., Smith, J. P., Werner, S., Chen, R., Roffer, M., Liu, Y., Muhling, B., Lindo-Atichati, D., Lamkin, J., Cerdeira-Estrada, S., and Enfield, D. B.: Natural variability of surface oceanographic conditions in the offshore Gulf of Mexico, *Prog. Oceanogr.*, 134, 54–76, 2015.
- New, A. L., Smeed, D. A., Czaja, A., Blaker, A. T., Mecking, J. V., Mathews, J. P., and Sanchez-Franks, A.: Labrador Slope Water connects the subarctic with the Gulf Stream, *Environ. Res. Lett.*, 16, 084019, <https://doi.org/10.1088/1748-9326/ac1293>, 2021.
- NOAA-GFDL: CEFI-regional-MOM6, GitHub [code], <https://github.com/NOAA-GFDL/CEFI-regional-MOM6> (last access: 22 June 2026), 2026.
- O’Neill, B. C., Tebaldi, C., van Vuuren, D. P., Eyring, V., Friedlingstein, P., Hurtt, G., Knutti, R., Kriegler, E., Lamarque, J.-F., Lowe, J., Meehl, G. A., Moss, R., Riahi, K., and Sanderson, B. M.: The Scenario Model Intercomparison Project (ScenarioMIP) for CMIP6, *Geosci. Model Dev.*, 9, 3461–3482, <https://doi.org/10.5194/gmd-9-3461-2016>, 2016.
- Park, J. and Sweet, W.: Accelerated sea level rise and Florida Current transport, *Ocean Sci.*, 11, 607–615, <https://doi.org/10.5194/os-11-607-2015>, 2015.
- Pershing, A. J., Alexander, M. A., Hernandez, C. M., Kerr, L. A., Le Bris, A., Mills, K. E., Nye, J. A., Record, N. R., Scannell, H. A., Scott, J. D., Sherwood, G. D., and Thomas, A. C.: Slow adaptation in the face of rapid warming leads to collapse of the Gulf of Maine cod fishery, *Science*, 350, 809–812, 2015.
- Pozo Buil, M., Jacox, M. G., Fiechter, J., Alexander, M. A., Bograd, S. J., Curchitser, E. N., Edwards, C. A., Rykaczewski, R. R., and Stock, C. A.: A Dynamically Downscaled Ensemble of Future Projections for the California Current System, *Frontiers Marine Sciences*, 8:612874, <https://doi.org/10.3389/fmars.2021.612874>, 2021.
- Roberts, M. J., Jackson, L. C., Roberts, C. D., Meccia, V., Docquier, D., Koenigk, T., Ortega, P., Moreno-Chamarro, E., Bellucci, A., Coward, A., Drijfhout, S., Exarchou, E., Gutjahr, O., Hewitt, H., Iovino, D., Lohmann, K., Putrasahan, D., Schiemann, R., Seddon, J., Terray, L., Xu, X., Zhang, Q., Chang, P., Yeager, S. G., Castruccio, F. S., Zhang, S., and Wu, L.:

- Sensitivity of the Atlantic Meridional Overturning Circulation to model resolution in CMIP6 HighResMIP simulations and implications for future changes, *J. Adv. Model. Earth Sy.*, 12, e2019MS002014, <https://doi.org/10.1029/2019MS002014>, 2020.
- Ross, A. C., Stock, C. A., Adcroft, A., Curchitser, E., Hallberg, R., Harrison, M. J., Hedstrom, K., Zadeh, N., Alexander, M., Chen, W., Drenkard, E. J., du Pontavice, H., Dussin, R., Gomez, F., John, J. G., Kang, D., Lavoie, D., Resplandy, L., Roobaert, A., Saba, V., Shin, S.-I., Siedlecki, S., and Simkins, J.: A high-resolution physical–biogeochemical model for marine resource applications in the northwest Atlantic (MOM6-COBALT-NWA12 v1.0), *Geosci. Model Dev.*, 16, 6943–6985, <https://doi.org/10.5194/gmd-16-6943-2023>, 2023.
- Ross, A. C., Stock, C. A., Koul, V., Delworth, T. L., Lu, F., Wittenberg, A., and Alexander, M. A.: Dynamically downscaled seasonal ocean forecasts for North American east coast ecosystems, *Ocean Sci.*, 20, 1631–1656, <https://doi.org/10.5194/os-20-1631-2024>, 2024.
- Rutherford, K., Fennel, K., Garcia Suarez, L., and John, J. G.: Uncertainty in the evolution of northwestern North Atlantic circulation leads to diverging biogeochemical projections, *Biogeosciences*, 21, 301–314, <https://doi.org/10.5194/bg-21-301-2024>, 2024.
- Saba, V. S., Griffies, S. M., Anderson, W. G., Winton, M., Alexander, M. A., Delworth, T. L., Hare, J. A., Harrison, M. J., Rosati, A., Vecchi, G. A., and Zhang, R.: Enhanced warming of the Northwest Atlantic Ocean under climate change, *J. Geophys. Res.-Oceans*, 121, 118–132, 2016.
- Sanchez-Franks, A. and Zhang, J.: Decadal variability and shifts of the Gulf Stream path, *J. Climate*, 28, 9825–9838, 2015.
- Seidov, D., Mishonov, A., and Parsons, R.: Recent warming and decadal variability of Gulf of Maine and Slope Water, *Limnol. Oceanogr.*, 66, 3472–3488, <https://doi.org/10.1002/lno.11892>, 2021.
- Sentman, L. T., Dunne, J. P., Horowitz, L. W., Naik, V., Paulot, F., Ginoux, P., and Zadeh, N.: Quantifying equilibrium climate sensitivity to atmospheric chemistry and composition representations in GFDL-CM4.0 and GFDL-ESM4.1, *Geophys. Res. Lett.*, 53, e2025GL116545, <https://doi.org/10.1029/2025GL116545>, 2026.
- Shevliakova, E., Malyshev, S., Martinez-Cano, I., Milly, P. C. D., Pacala, S. W., Ginoux, P., Dunne, K. A., Dunne, J. P., Dupuis, C., Findell, K. L., Ghannam, K., Horowitz, L. W., Knutson, T. R., Krasting, J. P., Naik, V., Phillipps, P., Zadeh, N., Yu, Y., Zeng, F., and Zeng, Y.: The land component LM4.1 of the GFDL Earth System Model ESM4.1: Model description and characteristics of land surface climate and carbon cycling in the historical simulation, *J. Adv. Model. Earth Sy.*, 16, e2023MS003922, <https://doi.org/10.1029/2023MS003922>, 2024.
- Shin, S. and Alexander, M. A.: Dynamical Downscaling of Future Hydrographic Changes over the Northwest Atlantic Ocean, *J. Climate*, 33, 2871–2890, <https://doi.org/10.1175/JCLI-D-19-0483.1>, 2020.
- Steinberg, J. M., Griffies, S. M., Krasting, J. P., Piecuch, C. G., and Ross, A. C.: A Link between U. S. East coast sea level and North Atlantic subtropical ocean heat content, *J. Geophys. Res.-Oceans*, 129, e2024JC021425, <https://doi.org/10.1029/2024JC021425>, 2024.
- Stock, C. A., Dunne, J. P., Fan, S., Ginoux, P., John, J., Krasting, J. P., Laufkötter, C., Paulot, F., and Zadeh, N.: Ocean Biogeochemistry in GFDL's Earth System Model 4.1 and Its Response to Increasing Atmospheric CO₂, *J. Adv. Model. Earth Sy.*, 12, e2019MS002043, <https://doi.org/10.1029/2019MS002043>, 2020.
- Stock, C. A., Dunne, J. P., Luo, J. Y., Ross, A. C., Van Oostende, N., Zadeh, N., Cordero, T. J., Liu, X., Teng, Y.-C.: Photoacclimation and photoadaptation sensitivity in a global ocean ecosystem model, *J. Adv. Model. Earth Sy.*, 17, e2024MS004701, <https://doi.org/10.1029/2024MS004701>, 2025.
- Tanaka, K. R., Torre, M. P., Saba, V. S., Stock, C. A., and Chen, Y.: An ensemble high-resolution projection of changes in the future habitat of American lobster and sea scallop in the Northeast US continental shelf, *Divers. Distrib.*, 26, 987–1001, <https://doi.org/10.1111/ddi.13069>, 2020.
- Volkov, D. L., Lee, S.-K., Domingues, R., Zhang, H., and Goes, M.: Interannual sea level variability along the southeastern seaboard of the United States in relation to whom it may concern: The gyre-scale heat divergence in the North Atlantic, *Geophys. Res. Lett.*, 46, 7481–7490, <https://doi.org/10.1029/2019GL083596>, 2019.
- Volkov, D. L., Zhang, K., Johns, W. E., Willis, J. K., Hobbs, W., Goes, M., Zhang, H., and Menemenlis, D.: Atlantic meridional overturning circulation increases flood risk along the United States southeast coast, *Nat. Commun.*, 14, 5095, <https://doi.org/10.1038/s41467-023-40848-z>, 2023.
- Volkov, D. L., Smith, R. H., Garcia, R. F., Smeed, D. A., Moat, B. I., Johns, W. E., and Baringer, M. O.: Florida Current transport observations reveal four decades of steady state, *Nat. Commun.*, 15, 7780, <https://doi.org/10.1038/s41467-024-51879-5>, 2024.
- Wang, Z., Boyer, T., Reagan, J., and Hogan, P.: Upper-Oceanic Warming in the Gulf of Mexico between 1950 and 2020, *J. Climate*, 36, 2721–2734, <https://doi.org/10.1175/JCLI-D-22-0409.1>, 2023.
- Wang, Z. A., Wanninkhof, R., Cai, W.-J., Byrne, R. H., Hu, X., Peng, T.-H., and Huang, W.-J.: The marine inorganic carbon system along the Gulf of Mexico and Atlantic coasts of the United States: Insights from a transregional coastal carbon study, *Limnol. Oceanogr.*, 58, 325–342, 2013.
- Wanninkhof, R., Barbero, L., Byrne, R., Cai, W.-J., Zhang, H. Z., Baringer, M., and Langdon, C.: Ocean acidification along the Gulf Coast and East Coast of the USA, *Cont. Shelf. Res.*, 98, 54–71, 2015.
- Weijer, W., Cheng, W., Garuba, O. A., Hu, A., and Nadiga, B. T.: CMIP6 models predict significant 21st century decline of the Atlantic Meridional Overturning Circulation, *Geophys. Res. Lett.*, 47, e2019GL086075, <https://doi.org/10.1029/2019GL086075>, 2020.
- Weinberg, J. R.: Bathymetric shift in the distribution of Atlantic surfclams: response to warmer ocean temperature, *ICES J. Mar. Sci.*, 62, 1444–1453, <https://doi.org/10.1016/j.icesjms.2005.04.020>, 2005.
- Worthington, L. V.: On the north Atlantic circulation, *John Hopkins Oceanographic Studies*, 6, 107–110, 1976.
- Yang, J. and Chen, K.: Profound changes in the seasonal cycle of sea level along the United States Mid-Atlantic Coast, *Geophys. Res. Lett.*, 52, e2024GL112273, <https://doi.org/10.1029/2024GL112273>, 2025.

- Yin, J., Schlesinger, M., and Stouffer, R.: Model projections of rapid sea-level rise on the northeast coast of the United States, *Nat. Geosci.*, 2, 262–266, <https://doi.org/10.1038/ngeo462>, 2009.
- Yuan, Y., Castelao, R. M., and He, R.: Variability in along-shelf and cross-shelf circulation in the South Atlantic Bight, *Cont. Shelf Res.*, 134, 52–62, <https://doi.org/10.1016/j.csr.2017.01.006>, 2017.
- Zantopp, R., Fischer, J., Visbeck, M., and Karstensen, J.: From interannual to decadal: 17 years of boundary current transports at the exit of the Labrador Sea, *J. Geophys. Res.-Oceans*, 122, 1724–1748, <https://doi.org/10.1002/2016JC012271>, 2017.
- Zhang, W., Alatalo, P., Crockford, T., Hirzel, A. J., Meyer, M. G., Oliver, H., Peacock, E., Petitpas, C. M., Sandwith, Z., Smith, W. O., Sosik, H. M., Stanley, R. H. R., Stevens, B. L. F., Turner, J. T., and McGillicuddy, D. J.: Cross-shelf exchange associated with a shelf-water streamer at the Mid-Atlantic Bight shelf edge, *Prog. Oceanogr.*, 210, 102931, <https://doi.org/10.1016/j.pocean.2022.102931>, 2023.
- Zhao, M., Golaz, J.-C., Held, I. M., Guo, H., Balaji, V., Benson, R., Chen, J. H., Chen, X., Donner, L. J., Dunne, J., Dunne, K. A., Durachta, J., Fan, S.-M., Freidenreich, S. M., Garner, S. T., Ginoux, P., Harris, L., Horowitz, L. W., Krasting, J. P., Langenhorst, A. R., Zhi, L., Lin, P., Lin, S. J., Malyshev, S., Mason, E., Milly, P. C. D., Ming, Y., Naik, V., Paulot, F., Paynter, D., Phillipps, P. J., Radhakrishnan, A., Ramaswamy, V., Robinson, T., Schwarzkopf, D., Seman, C. J., Shevliakova, E., Shen, Z., Shin, H. H., Silvers, L. G., Wilson, J. R., Winton, M., Wittenberg, A. T., Wyman, B., and Xiang, B.: The GFDL Global Atmosphere and Land Model AM4.0/LM4.0: 1. Simulation characteristics with prescribed SSTs, *J. Adv. Model. Earth Sy.*, 10, 691–734, <https://doi.org/10.1002/2017ms001208>, 2018a.
- Zhao, M., Golaz, J. C., Held, I. M., Guo, H., Balaji, V., Benson, R., Chen, J. H., Chen, X., Donner, L. J., Dunne, J. P., Dunne, K., Durachta, J., Fan, S. M., Freidenreich, S. M., Garner, S. T., Ginoux, P., Harris, L. M., Horowitz, L. W., Krasting, J. P., Langenhorst, A. R., Liang, Z., Lin, P., Lin, S. J., Malyshev, S. L., Mason, E., Milly, P. C. D., Ming, Y., Naik, V., Paulot, F., Paynter, D., Phillipps, P., Radhakrishnan, A., Ramaswamy, V., Robinson, T., Schwarzkopf, D., Seman, C. J., Shevliakova, E., Shen, Z., Shin, H., Silvers, L. G., Wilson, J. R., Winton, M., Wittenberg, A. T., Wyman, B., and Xiang, B.: The GFDL Global Atmosphere and Land Model AM4.0/LM4.0: 2. Model Description, Sensitivity Studies, and Tuning Strategies, *J. Adv. Model. Earth Sy.*, 10, 735–769, <https://doi.org/10.1002/2017MS001209>, 2018b.